HHS Public Access

Author manuscript

Neuron. Author manuscript; available in PMC 2019 January 17.

Published in final edited form as:

Neuron. 2018 January 17; 97(2): 434–449.e4. doi:10.1016/j.neuron.2017.12.022.

Nucleus accumbens subnuclei regulate motivated behavior via direct inhibition and disinhibition of VTA dopamine subpopulations

Hongbin Yang, **Johannes Willem de Jong**, **YeEun Tak**, **James Peck**, **Helen Bateup**, and **Stephan Lammel***

Department of Molecular and Cell Biology and Helen Wills Neuroscience Institute, University of California, Berkeley, 142 Life Science Addition #3200, CA 94720, USA

SUMMARY

Mesolimbic dopamine (DA) neurons play a central role in motivation and reward processing. Although the activity of these mesolimbic DA neurons is controlled by afferent inputs, little is known about the circuits in which they are embedded. Using retrograde tracing, electrophysiology, optogenetics and behavioral assays we identify principles of afferent-specific control in the mesolimbic DA system. Neurons in the medial shell subdivision of the nucleus accumbens (NAc) exert direct inhibitory control over two separate populations of mesolimbic DA neurons by activating different GABA receptor subtypes. In contrast, NAc lateral shell neurons mainly synapse onto ventral tegmental area (VTA) GABA neurons, resulting in disinhibition of DA neurons that project back to the NAc lateral shell. Lastly, we establish a critical role for NAc subregion-specific input to the VTA underlying motivated behavior. Collectively, our results suggest a distinction in the incorporation of inhibitory inputs between different subtypes of mesolimbic DA neurons.

eTOC Blurb

The mesolimbic dopamine system plays an important role in motivated behaviors, reinforcement learning, and reward processing. Yang et al. identify new functional and organizational principles of afferent-specific control in mesolimbic dopamine neurons that are critical for appetitive behaviors.

*Correspondence to: Stephan Lammel, Ph.D. (Lead Contact), 142 Life Science Addition #3200, University of California, Berkeley, Berkeley, CA 94720, USA, Telephone: 510-664-7821, lammel@berkeley.edu.

AUTHOR CONTRIBUTIONS

Stereotactic injections were performed by H.Y. Immunohistochemistry was performed by H.Y., H.T. and J.P. Electrophysiology was performed by H.Y. and J.J. Behavior experiments were performed by H.Y. and H.T. The study was designed by H.Y., H.B. and S.L. Results were analyzed and interpreted by H.Y. and S.L. The manuscript was written by H.Y. and S.L. and edited by all authors.

DECLARATION OF INTERESTS

The authors declare no competing interests.

Keywords

dopamine; GABA; mesolimbic; ventral tegmental area; nucleus accumbens; reward; motivation

INTRODUCTION

Dopamine (DA) projections from the ventral tegmental area (VTA) to the nucleus accumbens (NAc), which comprise the mesolimbic DA system (Bjorklund and Dunnett, 2007; Ikemoto, 2007; Morales and Margolis, 2017), play an important role in motivated behaviors, reinforcement learning, and reward processing (Hamid et al., 2015; Salamone and Correa, 2012; Schultz, 2016; Watabe-Uchida et al., 2017). Dysfunction of this system has been implicated in neuropsychiatric disorders such as substance abuse disorder (Ikemoto and Bonci, 2014; Lüscher, 2016) and depression (Nestler and Carlezon, 2006). While this has led to intense study into DA neurotransmission and the influence of DAergic input to the NAc on motivated behaviors, much less is known about the architecture and function of inhibitory feedback projections from the NAc to the VTA.

It is estimated that 50 – 70 % of all afferents to DA neurons are GABAergic and these inhibitory inputs have a major impact on the activity of DA neurons (Henny et al., 2012). Indeed, the removal of tonic inhibition from VTA DA neurons is considered an important candidate mechanism by which DA neurons may encode reward-related bursting (Paladini and Roeper, 2014; Watabe-Uchida et al., 2017) and by which drugs of abuse may cause increases in DA neuron activity (Ikemoto and Bonci, 2014; Lüscher, 2016). While direct inhibitory afferents to VTA DA neurons arise from a number of structures (Matsui et al., 2014), recent anatomical studies have shown that the NAc is a major source of such GABAergic input (Beier et al., 2015; Watabe-Uchida et al., 2012). By contrast, studies combining electrophysiology and optogenetic manipulations have failed to provide robust evidence for the existence of a direct inhibitory pathway from the NAc to DA neurons, suggesting that NAc inputs instead regulate VTA DA neurons through disinhibition (Bocklisch et al., 2013; Chuhma et al., 2011; Xia et al., 2011). Recently, Edwards and colleagues addressed these conflicting results by demonstrating that NAc neurons synapse onto both VTA GABA and DA neurons via selective activation of different GABA receptor subtypes ($GABA_A$ and $GABA_B$, respectively) (Edwards et al., 2017). However, questions about this circuit remain, as previous studies did not find evidence for $GABA_B$ receptor activation in VTA DA neurons in response to NAc stimulation (Xia et al., 2011). In addition, electrical stimulation of the striatum has been shown to induce inhibitory responses with very short latencies in DA neurons that are blocked by $GABA_A$ but not $GABA_B$ receptor antagonists, which hints at the presence of a direct pathway mediated by $GABA_A$ receptors instead (Paladini et al., 1999).

Concurrently with these studies, evidence has emerged suggesting that VTA DA neurons represent anatomically and functionally distinct populations, which project to different NAc subdivisions (medial shell (NAcMed), lateral shell (NAcLat), core) and receive highly biased inputs from separate ventral striatal subregions (Beier et al., 2015; Lammel et al., 2008, 2012). Because NAc subdivisions can exert opposing influences on motivated

behaviors (Aragona et al., 2008; Bassareo et al., 2002; Berridge and Kringelbach, 2015; Dreyer et al., 2016; Salamone and Correa, 2012) and subpopulations of VTA DA neurons presumably transmit different signals within these structures (Bromberg-Martin et al., 2010; Fields et al., 2007; Ikemoto, 2007; Lammel et al., 2014; Roeper, 2013), we hypothesized that separate NAc subdivisions are embedded into distinct VTA subcircuits. Determining the connectivity and function of distinct NAc inputs to the VTA would represent a critical step towards understanding the functional heterogeneity of VTA DA neurons and their role in motivated behaviors.

RESULTS

Anatomical organization of NAcMed and NAcLat inputs to the VTA

The NAc is composed of anatomically and functionally distinct subregions (medial shell (NAcMed), lateral shell (NAcLat) and core) and provides one of the most prominent projections to the VTA (Groenewegen et al., 1999; Ikemoto, 2007; Watabe-Uchida et al., 2012). We first characterized the anatomical organization of projections from the NAcMed and NAcLat to the VTA. We focused on the NAcMed and NAcLat since VTA DA neurons projecting to these regions demonstrate very different anatomical, molecular and electrophysiological properties (Lammel et al., 2008). Importantly, we could selectively express viral vectors in these areas without cross-contamination.

The principal cell types in the NAc are GABAergic medium spiny neurons (MSNs), which are divided into two groups based on their preferential expression of either D1- or D2-type DA receptors (Gerfen and Surmeier, 2011; Kupchik et al., 2015). Previous work has shown that D1- but not D2-expressing MSNs project to the VTA (Bocklisch et al., 2013; Edwards et al., 2017; Kupchik et al., 2015). To examine the innervation patterns from distinct NAc subdivisions, we targeted adeno associated viruses (AAVs) containing a double-floxed, inverted open reading frame for enhanced yellow fluorescent protein (AAV-DIO-eYFP) or mCherry (AAV-DIO-mCherry) to the NAcMed and NAcLat of the same D1-Cre mouse, respectively (Figures 1A and 1B). 6–8 weeks later, we sectioned the midbrain and observed that NAcMed and NAcLat terminals were located in different VTA subregions (Figure 1C). eYFP-expressing NAcMed terminals were predominantly located in the medial VTA (mVTA; paranigral nucleus and interfascicular nucleus), in close proximity to tyrosine hydroxylase (TH)-immunopositive neurons (i.e., DAergic neurons), and eYFP fluorescence levels were significantly higher in the mVTA compared to the lateral VTA (lVTA; lateral parabrachial nucleus). By contrast, NAcLat terminals were located mainly in the lVTA, with only a few NAcLat terminals near TH-immunopositive neurons, and fluorescence levels were significantly higher in the lVTA compared to the mVTA (Figures 1D and 1E; NAcMed: mVTA: 5.19 ± 0.75 %, lVTA: 0.17 ± 0.03 %, $p = 0.0026$; NAcLat: mVTA: 0.18 ± 0.06 %, lVTA: 3.18 ± 0.84 %, $p = 0.0237$; $n = 3$ mice). We also tested whether D2 MSNs, which selectively express adenosine2a (A2a) receptors, in the two NAc subdivisions project to the VTA. We injected AAVs conditionally expressing the two fluorophores into the NAcMed and NAcLat of A2a-Cre mice (Figures S1A and S1B). In this case, we did not detect eYFP or mCherry terminal expression in the VTA (Figure S1C). This distinct anatomical localization between NAcMed and NAcLat terminals in VTA subregions, which

are known to contain different mesolimbic DA subtypes (Lammel et al., 2008, 2011), suggests that the mesolimbic DA system comprises parallel reciprocal subcircuits (Figure 1F).

Mesolimbic DA subpopulations are embedded within distinct inhibitory networks

The segregated inputs from NAcMed and NAcLat to different subregions of the VTA indicate that inhibitory inputs to DA neurons in these subregions may be functionally distinct. To investigate this, we carried out dual retrograde tracing experiments by injecting green fluorescent retrobeads into NAcMed and red retrobeads into NAcLat into the same mouse and performed slice electrophysiology experiments (Figures 2A and 2B). Consistent with previous data (Lammel et al., 2008, 2011), we found that NAcLat-projecting DA neurons (identified by positive TH-immunoreactivity and red retrobead labeling) were located predominantly in the lVTA, while NAcMed-projecting DA neurons (TH-immunopositive and green retrobead labeling) clustered in the mVTA (Figure 2C). We then recorded miniature inhibitory postsynaptic currents (mIPSCs) from these two DA subpopulations (Figure 2D). Although no significant differences were observed in the amplitude of mIPSCs (Figure 2E; NAcLat-proj.: 42.77 ± 4.24 pA, n = 8; NAcMed-proj.: 38.18 ± 3.95 pA, n = 8; $p = 0.4414$), we found that the mIPSC frequency was significantly higher in NAcLat- compared to NAcMed-projecting VTA DA neurons (Figure 2F; NAcLat-proj.: 5.24 ± 0.63 Hz, n = 8; NAcMed-proj.: 1.22 ± 0.28 Hz, n = 8; $p < 0.0001$) indicating that inhibitory input differs remarkably between mesolimbic DA subpopulations. These findings are in agreement with a recent anatomical study, which reported that VTA DA neurons receive differential inputs from many brain structures known to have GABAergic projection neurons, including distinct NAc subdivisions (Beier et al., 2015).

NAcLat inputs promote disinhibition of NAcLat-projecting VTA DA neurons

We next combined optogenetics and slice electrophysiology to test whether distinct NAc subregions directly target different mesolimbic DA subpopulations. We first expressed channelrhodopsin-2 (ChR2) in the NAcLat and injected red fluorescent retrobeads into the NAcLat and NAcMed of the same animal (Figure 3A). We used the same fluorophore (i.e., rhodamine) to label both NAcMed- and NAcLat-projecting VTA DA neurons since green retrobeads would overlap with the ChR2-eFYP signal. We were able to reliably differentiate the two subtypes as they are located in different VTA subregions (Figure 2C; Lammel et al., 2008; 2011; 2012) and have different electrophysiological properties (Lammel et al., 2008, 2011). Using this approach, we could directly compare the synaptic strength and connectivity of NAc inputs to the two mesolimbic DA subpopulations. We recorded light-evoked inhibitory postsynaptic currents (IPSCs) from retrogradely labeled NAcMed- and NAcLat-projecting VTA neurons and verified the DA phenotype through post-hoc TH-immunohistochemistry of neurobiotin (NB) filled cells (Figure S2A). We found that relatively few NAcMed-projecting DA neurons responded to light stimulation (20.6 %, n = 7/34 cells), while the majority of cells that responded to light-stimulation were NAcLat-projecting DA neurons (61.5 %, n = 24/39 cells), and their mean amplitude was not significantly different (Figure 3B; NAcLat-proj.: 252.68 ± 40.51 pA, n = 24; NAcMed-proj.: 208.67 ± 50.64 pA, n = 7; $p = 0.5879$). Notably, light-evoked IPSCs were strongly reduced by 50 μM picrotoxin (PCTX), indicating the presence of a weak but direct $GABA_A$ receptor

(GABAAR)-mediated connection between the NAcLat and NAcLat-projecting DA neurons (Figure 3C; control: 235.7 ± 75.29 pA; PCTX: 54.35 ± 16.01 pA, n = 10; p = 0.0173). Because previous work suggested that the NAc mainly targets VTA GABA neurons (Bocklisch et al., 2013; Chuhma et al., 2011; Xia et al., 2011), we performed another series of experiments in which we compared light-evoked IPSCs between NAcLat-projecting DA neurons and non-DA (i.e., TH-immunonegative, no retrobead-labeling) neurons in the VTA. In this case, we found that the mean IPSC amplitude was significantly larger in non-DA neurons compared to NAcLat-projecting DA neurons (Figure 3D; NAcLat-proj.: 305.2 ± 64.42 pA, n = 13; non-DA.: 1675 ± 526 pA, n = 5; p = 0.0007). Our connectivity experiments revealed that NAc-Lat-projecting DA neurons and non-DA neurons both receive inhibitory inputs from NAcLat MSNs, with non-DA neurons receiving stronger inhibition on average. In order to determine the net effect of NAcLat MSN inputs on DA neuron activity, we recorded spontaneous firing of NAcLat-projecting DA neurons in the whole-cell current clamp configuration while optogenetically stimulating NAcLat terminals (20 Hz). We observed a significant increase in firing in response to NAcLat terminal stimulation in 90 % of the recorded cells (Figures 3E and 3F; off: 0.41 ± 0.09 Hz; 20 Hz: 1.53 ± 0.26 Hz, off: 0.37 ± 0.08 pA, n = 20; RM one-way ANOVA, $p_{off\ vs.\ on} = 0.0002$, $p_{off\ vs.\ off} = 0.5163$, $p_{on\ vs.\ off} = 0.0004$). Thus, despite the presence of a modest direct inhibitory connection, activating NAcLat terminals ultimately results in disinhibition of NAcLat-projecting DA neurons, most likely via inhibition of local GABAergic neurons within the VTA.

NAcMed inputs directly inhibit NAcMed-projecting VTA DA neurons

To investigate the consequences of activating NAcMed inputs to the VTA, we expressed ChR2 in the NAcMed and injected red retrobeads into NAcLat and NAcMed of the same animal and recorded from different mesolimbic DA subpopulations in the VTA (Figures 3G and S2B). Surprisingly, we detected large light-evoked IPSCs in 83 % (n = 15/18 cells) of NAcMed-projecting DA neurons that were blocked by PCTX (Figures 3H and I, control: 1508 ± 324.9 pA; PCTX: 235 ± 68.5 pA, n = 6; p = 0.0129), suggesting the existence of a strong monosynaptic connection between the NAcMed and NAcMed-projecting DA neurons that is mediated by GABAARs. In fact, the mean IPSC amplitude was over four times larger than the relatively weak direct reciprocal connectivity of the NAcLat pathway. By contrast, the proportion of NAcLat-projecting DA neurons receiving NAcMed input was substantially lower (19 %, n = 7/36 cells) and their mean IPSC amplitude was significantly smaller compared to NAcMed-projecting DA neurons (Figure 3H; NAcMed-proj.: 1110.75 ± 194.72 pA, n = 15; NAcLat-proj.: 357.7 ± 74.89 pA, n = 7; p = 0.018). We also detected light-evoked IPSCs in non-DA neurons in the VTA. Their mean IPSC amplitude was not significantly different from NAcMed-projecting DA neurons (Figure 3J; NAcMed-proj.: 639.1 ± 175.3 pA, n = 10; non-DA: 1291 ± 470.9 pA, n = 7; p = 0.161). Lastly, spontaneous firing of the majority (> 70 %) of NAcMed-projecting DA neurons was inhibited by 20 Hz optogenetic stimulation of NAcMed terminals in the VTA (Figures 3K and 3L; off: 1.48 ± 0.22 Hz; 20 Hz: 0.71 ± 0.24 Hz, off: 1.43 ± 0.24 Hz, n = 17; RM one-way ANOVA, $p_{off\ vs.\ on} = 0.0258$, $p_{off\ vs.\ off} = 0.9054$, $p_{on\ vs.\ off} = 0.0298$). Combined, these results suggest that NAcMed inputs preferentially exert direct inhibitory control over non-DA neurons, and over NAcMed-projecting DA neurons, and that the latter inhibition is mediated by GABAARs.

NAcLat inputs to VTA GABA neurons are stronger than NAcMed inputs

Both NAcLat and NAcMed make robust synaptic connections onto non-DA neurons in the VTA (Figures 3D and 3J). Because the VTA contains heterogeneous populations of DAergic, GABAergic and glutamatergic neurons (Fields et al., 2007; Lammel et al., 2014; Morales and Margolis, 2017), we next investigated the synaptic connectivity between NAcLat and NAcMed and genetically-identified VTA GABA neurons. To do this, we expressed ChR2 in the NAcLat or NAcMed of GAD2::tdTomato (GAD2-tdT) mice and recorded light-evoked IPSCs in GAD2-tdT-positive neurons throughout the VTA (Figure S2C). We detected robust light-evoked IPSCs in GAD2-tdT-positive neurons in response to both NAcMed and NAcLat terminal stimulation; however, connections from NAcLat to VTA GAD2-tdT-positive neurons were significantly stronger and caused larger IPSCs (Figures S2D and S2E; NAcLat: 1665 ± 365.2 pA, n = 23; NAcMed: 734.6 ± 223.24 pA, n = 23; p = 0.0352). Importantly, response rates were higher when we recorded GAD2-tdT-positive neurons in a VTA subregion that was matched with the corresponding NAc subdivision, i.e., mVTA for NAcMed and lVTA for NAcLat terminal stimulation (Figure S2F; NAcMed: mVTA: 92 %, n = 12/13 cells, lVTA: 46 %, n = 11/24 cells; NAcLat: mVTA: 36 %, n = 4/11 cells, lVTA: 79 %, n = 19/24 cells), consistent with the subregion-specific location of NAcMed and NAcLat terminals in the VTA (Figures S2G and S2H).

Given the subregion-specific innervation of VTA GABA neurons by the NAc, we next asked whether there are differences in their inhibitory synaptic control over NAcMed- and NAcLat-projecting DA neurons. To investigate this, we injected AAV-DIO-ChR2 into the VTA of GAD2-Cre mice and recorded from retrogradely labeled NAcMed- and NAcLat-projecting DA neurons (Figure S2I). Optogenetic stimulation of VTA GABA neurons evoked GABAAR-mediated IPSCs in both NAcMed- and NAcLat-projecting DA neurons. However, IPSCs were significantly larger in NAcLat-projecting DA neurons than in NAcMed-projecting DA neurons (Figure S2J; NAcMed-proj.: 628.6 ± 111.5 pA, n = 13; NAcLat-proj.: 1516 ± 195.8 pA, n = 11; p = 0.0005). Together, these findings suggest that NAcMed and NAcLat projections form distinct inhibitory subcircuits in the VTA incorporating different populations of GABAergic and mesolimbic DA neurons with opposing effects on the net activity of VTA DA neurons.

Optogenetic control of NAcLat and NAcMed inputs to VTA in freely moving mice

DA neurons in the lVTA form a largely homogeneous cell population that promote reward and reinforcement (Eshel et al., 2016; Schultz, 2016; Steinberg and Janak, 2013) and activation of NAcLat inputs to the VTA results in disinhibition of lVTA DA neurons (Figures 3D–3F). Thus, we hypothesized that activation of NAcLat terminals in the VTA produces reward-related behaviors. To test our prediction, we injected AAV-DIO-ChR2 or a control vector, AAV-DIO-eYFP, into the NAcLat of D1-Cre mice, implanted an optical fiber above the VTA and performed a real-time place preference assay (Figures 4A, 4B and S3). Consistent with our anatomical characterization of NAcLat inputs (Figure 1), we observed ChR2-expressing NAcLat terminals mainly in the lVTA (Figure 4C). The results from our behavioral experiments were consistent with our hypothesis. Optogenetic stimulation of NAcLat inputs in the VTA caused robust real-time place preference, where animals spent significantly more time in the compartment where they received light stimulation and less

time in the compartment where they did not receive stimulation. Indeed, switching the stimulation to the originally non-stimulated compartment caused immediate reversal of compartment preference (Figures 4D–4F; non-stim.: 184.4 ± 27.16 s, stim.: 894.9 ± 40.69 s, n = 9; $p < 0.0001$). We also observed a significant increase in the total number of entries into the stimulated compartment (Figure 4G; non-stim.: 14 ± 1.19, stim.: 32.22 ± 4.54, n = 9; p = 0.0038). Mice that received injection of the control vector (AAV-DIO-eYFP) into the NAcLat spent equal amounts of time on either side of the chamber (data not shown). Furthermore, activation of NAcLat VTA inputs supported robust reinforcement in an intracranial self-stimulation task where mice could respond at a nosepoke port to obtain stimulation (Figure 4H; ChR2: 1523 ± 316.4, n = 9, eYFP: 25.5 ± 7.84, n = 6; p = 0.0021). Optogenetic stimulation of NAcLat inputs had no significant effect on either anxiety-related behavior assessed in the elevated plus maze (Figure 4I; off: 9.11 ± 2.64 s, on: 3.32 ± 0.97 s, off: 10.47 ± 4.37 s, n = 8; RM one-way ANOVA, $p_{off\ vs.\ on} = 0.2473$, $p_{off\ vs.\ off} = 0.9662$, $p_{on\ vs.\ off} = 0.2688$) or general locomotor activity assessed in the open field test (Figure S4A). Next, we sought to test whether silencing NAcLat terminals in the VTA influences place preference behavior and hypothesized that this manipulation will induce aversion behavior. We observed a small but not significant effect on place avoidance behavior when inhibiting NAcLat terminals in the VTA using an inhibitory opsin (halorhodopsin, eNpHR3.0; Figure S5). Such a weak effect is surprising given that we had initially observed a strong and robust effect when driving NAcLat terminals in the VTA using ChR2. While these negative results could imply that NAcLat inputs to the VTA are not causally involved in this behavior, we think that this is relatively unlikely because of potential difficulties in generating changes in neurotransmitter release with terminal inhibition (Howe and Dombeck, 2016; Mahn et al., 2016). Thus, it is likely that the inability to suppress a large enough portion of NAcLat terminals in the VTA contributes to the lack of place aversion behavior in this experiment.

We next investigated the functional role of NAcMed inputs to the VTA by injecting AAV-DIO-ChR2 or AAV-DIO-eYFP into the NAcMed of D1-Cre mice and implanting an optical fiber above the VTA (Figures 5A, 5B and S3). As expected, ChR2-expressing NAcMed terminals were located mainly in the mVTA (Figure 5C). Based on our finding that NAcMed inputs exert strong inhibitory influence over NAcMed-projecting DA neurons (Figures 3K and 3L), we predicted that optogenetic stimulation of NAcMed inputs will induce aversion. Surprisingly, optogenetic stimulation of NAcMed inputs elicited neither immediate aversion nor preference and did not support intracranial self-stimulation (Figures 5D–5G; place preference: non-stim.: 350.6 ± 53.74 s, stim.: 325.8 ± 35.59 s, n = 10; p = 0.6897; self-stimulation: ChR2: 45 ± 6.06, n = 10, eYFP: 32.33 ± 5.8, n = 6; p = 0.184). Instead, we observed that after switching the stimulation to the original non-stimulated compartment in our three-chamber place preference assay, the mice showed a strong preference for the neutral area (Figures 5D and 5E). In fact, the total time spent in the neutral area was significantly higher when compared to control animals or in response to optogenetic stimulation of ChR2-expressing NAcLat inputs (Figure 5H; NAcMed: ChR2: 523.5 ± 68.58 s, n = 10, eYFP: 293.5 ± 64.55 s, n = 6; NAcLat: ChR2: 82.53 ± 9.02 s, n = 9, eYFP: 304.9 ± 42.22 s; n = 8; two-way ANOVA (interaction), p = 0.0002; NAcMed p = 0.0097, NAcLat p = 0.0097). Although arguments can be made that the increase in time spent in the neutral

area reflects aversion, this phenotype was clearly different from the aversion previously observed in response to optogenetic stimulation of lateral habenula (LHb) inputs to the VTA (Lammel et al., 2012, 2015; Stamatakis and Stuber, 2012). Optogenetic stimulation of NAcMed inputs had no acute effect on anxiety or locomotion, but we noticed that immediately after turning off light stimulation, the mice showed increased anxiety levels (Figure 5I; off: 10.52 ± 3.83 s, on: 9.52 ± 3.38 s, off: 1.9 ± 1.1 s, n = 10; RM one-way ANOVA, $p_{off\ vs.\ on} = 0.9191$, $p_{off\ vs.\ off} = 0.0664$, $p_{on\ vs.\ off} = 0.0484$) and a reduction in general locomotor activity (Figure S4B). These effects were not observed in the control group (eYFP; data not shown), or in response to NAcLat (Figures 4I and S4A) or LHb (Lammel et al., 2012) terminal stimulation in the VTA.

Thus, optogenetic stimulation of VTA afferents that originate from distinct NAc subnuclei induces distinct behavioral phenotypes. Activation of NAcLat inputs resulted in a robust reinforcement phenotype, while stimulation of NAcMed terminals produced a subsequent, generalized state of behavioral suppression that followed the stimulation period, and this was not specific to reward or to aversion.

NAcMed inputs control NAcLat-projecting DA neurons via $GABA_B$ receptors

The observation that optogenetic stimulation of NAcMed inputs does not promote reward or aversion is puzzling. We revisited the literature in light of our unexpected behavioral findings to look for something that could explain this discrepancy. GABAergic inhibition of VTA DA neurons is mediated by both fast ionotropic GABAARs and slow metabotropic $GABA_B$ receptors (GABABRs) (Cruz et al., 2004; Labouèbe et al., 2007). A recent study showed that NAc inputs to the VTA inhibit the firing of DA neurons in the lVTA through specific activation of GABABRs (Edwards et al., 2017). Based on these findings, we speculated that NAcMed inputs do not only inhibit NAcMed-projecting DA neurons through GABAARs (Figures 3H and 3I), but they may also activate GABABRs in NAcLat-projecting DA neurons in the lVTA. Thus, the behavioral phenotype we observed in response to NAcMed terminal stimulation in the VTA (Figure 5) may involve inhibition of mesolimbic DA subpopulations through separate GABA receptor classes.

Because relatively little is known about GABABR-mediated function in projection-defined DA subpopulations, we first examined the effects of GABABR-activation in NAcLat- and NAcMed-projecting DA neurons (Figure 6A). To do this, we performed whole-cell recordings from the two mesolimbic subtypes and bath applied the GABABR agonist baclofen (*p*-chlorophenyl-GABA). As shown previously for I_h-positive VTA DA neurons (Cruz et al., 2004; Labouèbe et al., 2007), we found that application of 100 μM baclofen evoked robust outward currents in bead-labeled NAcLat-projecting DA neurons that correlated with a decrease in input resistance (data not shown), showed a characteristic acute desensitization and was inhibited with a GABABR antagonist (100 μM CGP35348). In contrast, baclofen-activated currents were significantly smaller in NAcMed-projecting DA neurons (Figures 6B and 6C; NAcLat-proj.: 102.4 ± 20.59 pA, n =7; NAcMed-proj.: 12.95 ± 5.06 pA, n = 6; p = 0.0024). The VTA also contains glutamatergic neurons, and co-expression of glutamatergic markers (i.e., VGLUT2) has been reported in DA neurons (Morales and Margolis, 2017). Interestingly, we found that VGLUT2 is predominantly co-

expressed in NAcMed-projecting DA neurons, but can only be detected in very few NAcLat-projecting DA neurons (Figures S6A–6F). To investigate the possibility of GABABR-mediated transmission in VTA glutamatergic neurons, we performed whole-cell patch clamp recordings from VTA glutamatergic neurons (i.e., VGLUT2+ TH−) and VGLUT2-coexpressing VTA DA neurons (i.e., VGLUT2+ TH+) and applied 100 μM baclofen (Figures S6G–6K). We found that baclofen-evoked peak outward currents in these two cell populations were comparable to currents observed in NAcMed-projecting DA neurons, but ~3–5 times smaller than in NAcLat-projecting DA neurons (Figures S6H and S6I).

To examine afferent-specific GABABR-mediated currents, we injected AAV-DIO-ChR2 into the NAcMed of D1-Cre mice and performed whole-cell recordings from NAcLat- and NAcMed-projecting DA neurons (Figure 6D). In voltage clamp, trains of stimuli (20 Hz, 20 pulses) produced slow light-evoked IPSCs in NAcLat-projecting DA neurons in 18 out of 34 recorded cells. The IPSCs had a similar waveform as the GABABR-mediated IPSCs observed by (Edwards et al., 2017) and were blocked by bath application of 100 μM CGP35348 (Figures 6E and 6F; ACSF: 13.24 ± 2.57 pA, n = 18; CGP35348: 0.3 ± 0.11 pA, n = 8; p = 0.0028). In addition, 20 Hz light stimulation of NAcMed terminals reduced spontaneous firing of NAcLat-projecting DA neurons in 7 out of 20 recorded cells, which was blocked by bath application of 100 μM CGP35348 (Figure 6G; off: 0.54 ± 0.08 Hz; ACSF: 0.15 ± 0.04 Hz; CGP: 0.65 ± 0.1 Hz, n = 7; RM one-way ANOVA, $p_{off\ vs.\ ACSF}$ = 0.0066, $p_{off\ vs.\ CGP}$ = 0.4306, $p_{ACSF\ vs.\ CGP}$ = 0.0081). In contrast, light stimulation of NAcMed terminals generally failed to produce slow light-evoked IPSCs in NAcMed-projecting DA neurons (Figure 6E; only 1 out of 15 recorded cells produced an 8.1 pA response) and bath application of 100 μM CGP35348 did not influence the inhibition of spontaneous firing evoked by NAcMed terminal stimulation in these cells (Figure 6H; off: 1.42 ± 0.16 Hz; ACSF: 0.29 ± 0.21 Hz; CGP: 0.3 ± 0.18 Hz, n = 10; RM one-way ANOVA, $p_{off\ vs.\ ACSF}$ = 0.0004, $p_{off\ vs.\ CGP}$ = 0.0004, $p_{ACSF\ vs.\ CGP}$ = 0.994). No slow light-evoked GABABR-mediated responses were detected in either NAcLat- or NAcMed-projecting DA neurons when ChR2 was expressed in the NAcLat (Figures S7A and S7B) and bath application of 100 μM CGP35348 did not influence the effects of light stimulation of NAcLat terminals on spontaneous firing of NAcLat- and NAcMed-projecting DA neurons (Figures S7C and S7D). Together, these findings indicate that D1 MSNs in the NAcMed selectively inhibit NAcLat-projecting DA neurons through GABABR activation.

The ability to elicit GABABR-mediated responses in NAcLat-projecting DA neurons (Figures 6E and 6F) and GABAAR-mediated responses in NAcMed-projecting DA neurons (Figures 3B and 3C) suggests that the behavioral phenotype we observed in response to NAcMed terminal stimulation (Figure 5) might be due to a strong overall suppression of both mesolimbic subsystems. To formally test this possibility, we expressed ChR2 in the NAcMed of D1-Cre mice and implanted opto-fluid cannulas, which allow both light stimulation and infusion of fluids, just dorsal to the VTA (Figures 7A and S8). We then optogenetically stimulated NAcMed inputs in a real-time place preference assay, but 3-min before the experiment we infused either artificial cerebrospinal fluid (ACSF) or the GABABR antagonist CGP35348 into the VTA (Figure 7B). Infusion of ACSF resulted in the same behavior we observed previously (Figure 7C; non-stim.: 365.3 ± 28.30 s, stim. side: 439.7 ± 72.11s, n = 6; p = 0.4353). In contrast, infusion of 15 nM CGP35348 produced

place preference behavior in all mice tested (Figure 7D; non-stim.: 296.8 ± 42.61 s, stim.: 617.8 ± 55.76 s, n = 6; $p < 0.0001$). Moreover, CGP35348 infusion also prevented the increase in anxiety behavior which we observed immediately after turning off light stimulation in ACSF-treated animals (Figures 7E and 7F; ACSF: off: 31.93 ± 9.5 s, on: 32.07 ± 7.86 s, off: 8.6 ± 4.41 s; n = 6; RM one-way ANOVA, $p_{off\ vs.\ on} = 0.9996$, $p_{off\ vs.\ off} = 0.0203$, $p_{on\ vs.\ off} = 0.0219$; CGP35348: off: 46.4 ± 18.48 s, on: 32.85 ± 9.37 s, off: 54.08 ± 22.87 s, n = 6; RM one-way ANOVA, $p_{off\ vs.\ on} = 0.4417$, $p_{off\ vs.\ off} = 0.5688$, $p_{on\ vs.\ off} = 0.435$). Together, these findings reveal a subcircuit for motivated behaviors that involves D1 MSNs in the NAcMed, which selectively inhibit distinct mesolimbic DA subpopulations through different classes of GABA receptors.

DISCUSSION

Here, we have used a multidisciplinary approach combining retrograde tracing, electrophysiology, optogenetics and behavioral assays to elucidate the circuit architecture and function of reciprocal connectivity in the mesolimbic DA system. A prominent finding of our study is that D1-expressing MSNs in the NAcMed exert direct inhibitory control over two distinct mesolimbic DA subpopulations by activating separate GABA receptor subtypes. Specifically, D1-expressing MSNs in the NAcMed preferentially inhibit NAcMed-projecting DA neurons via GABAAR and NAcLat-projecting DA neurons via GABABR. In contrast, D1-expressing MSNs in the NAcLat mainly synapse onto VTA GABA neurons resulting in a disinhibition of NAcLat-projecting DA neurons (Figure 8). Moreover, using *in vivo* optogenetic manipulations we established a critical role for NAc subregion-specific inputs to the VTA in regulating motivated behaviors.

Our findings help to solve an ongoing controversy regarding the connectivity of the NAc with VTA subpopulations. While recent anatomical studies suggest that the largest proportion of monosynaptic inputs to VTA DA neurons originates from the NAc (Beier et al., 2015; Faget et al., 2016; Watabe-Uchida et al., 2012), which is mainly composed of GABAergic MSNs, studies combining electrophysiology and optogenetic manipulations have failed to provide compelling evidence for the existence of a direct inhibitory synaptic connection to DA neurons (Bocklisch et al., 2013; Chuhma et al., 2011; Xia et al., 2011). However, in light of mounting evidence pointing to anatomical and functional heterogeneity between subpopulations of VTA DA neurons, a major limitation of these functional studies is that the connection between the NAc and VTA neurons has been investigated in the absence of subregion and/or projection specificity. It is likely that these studies focused on NAcMed inputs to I_h-positive DA neurons in the lateral VTA, which indeed are very sparse compared to NAcMed inputs to NAcMed-projecting DA neurons. By differentiating VTA DA neurons based on their specific afferent and efferent connectivity, we were able to confirm a striking reciprocal connectivity between the NAcMed and its DAergic inputs, thereby mirroring the results of recent transsynaptic rabies virus tracing studies (Beier et al., 2015; Faget et al., 2016; Watabe-Uchida et al., 2012). Thus, our results bridge the gap between previously confounding electrophysiological and anatomical studies that have controversially discussed the existence of direct monosynaptic connections between the NAc and VTA DA neurons.

Our input- and projection-specific optogenetic experiments not only provide functional information about connection probability and strength between distinct NAc subregions and VTA subpopulations, but also help to elucidate the specific contribution of GABAARs and GABABRs in these pathways. The prevailing view is that GABAAR activation (e.g., through infusion of muscimol into the VTA or optogenetic activation of VTA GABA neurons) results in increased firing of VTA DA neurons through disinhibition (Bocklisch et al., 2013; Kalivas et al., 1990; Klitenick et al., 1992; Tan et al., 2012; van Zessen et al., 2012). Nevertheless, several studies observed “paradoxical” effects in response to GABAAR activation that resulted in decreased DA transmission (Ikemoto et al., 1998; Westerink et al., 1996). Such results may reflect dose-dependent effects due to differences in sensitivity of GABAARs on VTA DA and GABA neurons (Doherty and Gratton, 2007) or, based on our data, on GABAAR activation in different mesolimbic subsystems. Accordingly, VTA GABAAR activation could result in an increase in DA transmission in the NAcLat via disinhibition of NAcLat-projecting DA neurons and a decrease in DA transmission in the NAcMed due to direct suppression of DA neurons projecting to NAcMed.

It has been suggested that within the VTA, GABAARs and GABABRs are anatomically and functionally dissociable (Cameron and Williams, 1993; Doherty and Gratton, 2007; Klitenick et al., 1992; Laviolette and Van Der Kooy, 2001; Panagis and Kastellakis, 2002; Sugita et al., 1992; Xi and Stein, 1998). This widely held assumption has gained momentum with a recent study showing that NAc neurons inhibited VTA GABA neurons through GABAARs and inhibited VTA DA neurons via GABABRs (Edwards et al., 2017). Our data is consistent with this finding, yet it shows that our perspective of GABA signaling in the VTA needs to be more nuanced; specifically, limiting GABAAR and GABABR-mediated actions to VTA GABA neurons and DA neurons, respectively, is an oversimplification. In contrast, we find distinct GABAAR-mediated pathways that originate from discrete NAc subregions and target specific VTA DA and GABA subpopulations. Such parallel channels for information flow are reminiscent of the parallel nigrostriatal DA subcircuits recently described for different subregions of the substantia nigra (Lerner et al., 2015). Nevertheless, NAcMed and NAcLat do not exclusively form parallel pathways to the VTA. We also found that there is remarkable cross communication between these systems; in addition to targeting NAcMed-projecting DA neurons via GABAARs, the NAcMed also exert strong inhibitory influence over NAcLat-projecting DA neurons that is mediated through GABABR activation. It is currently unknown whether these inputs originate from the same D1-expressing MSNs or from separate cell populations, and whether neurons in the NAcMed and NAcLat directly communicate with each other. However, the information flow from medial to lateral described here for the mesolimbic DA system and in (Lerner et al., 2015) for the nigrostriatal DA system provides new insights into the ascending spiral model originally described by (Haber et al., 2000).

What is the functional role of NAc inputs to the VTA? The removal of tonic inhibition from VTA GABA neurons onto DA neurons is a critical candidate mechanism by which DA neurons could encode reward-related bursting (Paladini and Roeper, 2014; Watabe-Uchida et al., 2017) and by which drugs of abuse exert maladaptive increases in DA neuron activity (Ikemoto and Bonci, 2014; Lüscher, 2016). Given that the NAc is a major source of input to VTA GABA neurons (Bocklisch et al., 2013; Faget et al., 2016; Kalivas et al., 1993; Watabe-

Uchida et al., 2012; Xia et al., 2011), it is somewhat surprising that reward-related behaviors by direct optogenetic stimulation of NAc terminals in the VTA had not been previously demonstrated. We suspect that the absence of reporting on NAc terminal stimulation using optogenetic manipulations may be due to the fact that researchers have focused on the NAcMed, which as we demonstrate, produces a generalized state of behavioral suppression instead of reward and is therefore not consistent with the disinhibition model. Instead, only when selectively stimulating NAcLat terminals in the VTA were we able to successfully induce a potent reward phenotype, which is likely caused by a disinhibition of NAcLat-projecting VTA DA neurons. However, other contributing factors such as the modulation of VTA GABA projection neurons (Laviolette and Van Der Kooy, 2001) or co-release of neuropepetides from the NAcLat (Xia et al., 2010) cannot be excluded. In contrast, when stimulating NAcMed terminals in the VTA, a reward phenotype is revealed only after infusion of the GABABR antagonist CGP35348 into the VTA. Activation of GABABRs in the VTA (e.g., through infusion of baclofen) has a reward-suppressing effect (Willick and Kokkinidis, 1995) and decreases DA output in the NAc (Pitman et al., 2014; Westerink et al., 1996; Xi and Stein, 1998). Thus, NAcLat-projecting DA neurons are under strong, sustained inhibition from both long-range and local inputs, which is reflected in their high mIPSC frequency (Figure 2); this might be necessary for an effective tonic suppression of DA neuron activity in the absence of salient or reward-predicting stimuli (Henny et al., 2012). Surprisingly, however, infusion of CGP35348 into the VTA induced a reward phenotype when stimulating NAcMed terminals in the VTA (Figure 7). If the rewarding phenotype after GABABR blockade is indeed caused by an inhibition of NAcMed-projecting DA neurons, which was the predominant net effect when activating these inputs, then this points to a fundamentally different role of NAcMed-projecting DA neurons underlying motivated behaviors. However, it is also possible that optogenetic manipulations of NAc terminals in the VTA may result in backpropagating action potentials that activate other brain structures via axon collaterals. In addition, our stimulation pattern may not recapitulate physiological activity patterns in NAc neurons projecting to the VTA. Lastly, it is interesting that VGLUT2 is strongly co-expressed in NAcMed-projecting DA neurons (Figure S6). Thus, future studies need to delve deeper into the functional role of DA and glutamate co-release in the NAcMed. Despite these limitations, our results suggest that our perspective of the mesolimbic DA system needs to be more nuanced than traditional views that have often considered these cells as a homogenous population. Emerging data requires that we develop a new perspective on this circuitry that will guide future treatment strategies for addiction and other neuropsychiatric disorders where dysfunction of the neural systems underlying motivated behaviors have been strongly implicated.

STAR METHODS

CONTACT FOR REAGENT AND RESOURCE SHARING

Further information and requests for resources and reagents should be directed to and will be fulfilled by the Lead Contact Stephan Lammel (lammel@berkeley.edu).

EXPERIMENTAL MODEL AND SUBJECT DETAILS

The following mouse lines (25–30 g, 8–12 weeks old, males and females were counterbalanced across conditions with no significant effects of sex observed) were used for the experiments: C57Bl6 mice (Jackson Laboratory), D1-Cre (GENSAT, stock number: 017264-UCD, strain code: Tg(Drd1-cre)EY262Gsat/Mmucd), A2a-Cre (GENSAT, stock number: 017263-UCD, strain code: Tg(Drd2-cre)ER44Gsat/Mmucd), GAD2-IRES-Cre (Jackson Laboratory, stock number: 010802, strain code: Gad2$^{tm2(cre)Zjh}$/J), VGLUT2::IRES-Cre (Jackson Laboratory, stock number: *016963*, strain code: Slc17a6tm2(cre)Lowl/J), Ai14 Cre reporter mice (Jackson Laboratory, stock number: 007908, strain code: B6;129S6 Gt(ROSA)26Sor$^{tm14(CAG-tdTomato)Hze}$/J). Ai14 Cre reporter mice were crossed to GAD2-IRES-Cre mice. Mice were maintained on a 12:12 light cycle (lights on at 07:00). All procedures complied with the animal care standards set forth by the National Institutes of Health and were approved by University of California Berkeley's Administrative Panel on Laboratory Animal Care.

METHOD DETAILS

STEREOTAXIC SURGERIES—As previously described (Lammel et al., 2008; 2012; 2015) all stereotaxic injections were performed under general ketamine–dexmedetomidine anesthesia and using a stereotaxic instrument (Kopf Instruments, Model 1900). For red/green fluorescent retrobead labeling, mice were injected unilaterally with fluorescent retrobeads (100 nl; LumaFluor Inc.) in the Nucleus accumbens (NAc) medial shell (NAcMed, bregma: 1.50 mm, lateral: 0.55 mm, ventral: −4.70 mm) and/or NAc lateral shell (NAcLat, bregma: 0.98 mm, lateral: 1.80 mm, ventral: −4.92 mm) using a 1 μl Hamilton syringe (Hamilton). The AAVs (adeno associated virus) used in this study were from the Deisseroth laboratory (AAV5-hSyn-hChR2(H134R)-eYFP; AAV5-EF1α–DIO-hChR2(H134R)-eYFP; AAV5-EF1α-DIO-eYFP; AAV5-EF1α-DIO-mCherry; AAV5-EF1α-DIO-eNpHR3.0-eYFP; ~10^{12} infectious units per ml, prepared by the University of North Carolina Vector Core Facility). For viral injections, 300 nl of concentrated AAV solution was injected into the NAc lateral shell and/or NAc medial shell (same coordinates as above) or the ventral tegmental area (VTA; bregma: −3.40 mm, lateral: 0.40 mm, ventral: −−4.30 mm) using a syringe pump (Harvard Apparatus) at 150 nl/min. The injection needle was withdrawn 10 min after the end of the infusion. For behavioral experiments, Channelrhodopsin-2 (ChR2)-injected mice received unilateral implantation of a chronically implanted optical fiber (NA = 0.37; Newdoon Inc.) dorsal to the VTA (bregma: −3.40 mm, lateral: 0.40 mm, ventral: −3.90 mm). One layer of adhesive cement (C&B Metabond; Parkell) followed by cranioplastic cement (Dental cement) was used to secure the fiber to the skull. The incision was closed with a suture and tissue adhesive (Vetbond; 3M). The animal was kept on a heating pad until it recovered from anesthesia. Experiments were performed 6–8 weeks (for AAVs) or 2–7 days (for retrobeads) after stereotactic injection. Injection sites and optical fiber placements were confirmed in all animals by preparing coronal sections (50–100 μm) of injection and implantation sites. We routinely carried out complete serial analyses of the injection sites and optical fiber placements (Figures S3 and S8). Although optical fiber placements varied slightly from mouse to mouse, behavioral data from all mice were included in the study.

ELECTROPHYSIOLOGY—Mice were deeply anaesthetized with pentobarbital (200 mg/kg ip; Vortech). Coronal midbrain slices (200 μm) were prepared after intracardial perfusion with ice-cold artificial cerebrospinal fluid (ACSF) containing (in mM) 50 sucrose, 125 NaCl, 25 $NaHCO_3$, 2.5 KCl, 1.25 NaH_2PO_4, 0.1 $CaCl_2$, 4.9 $MgCl_2$, and 2.5 glucose (oxygenated with 95% O_2/5% CO_2). After 90 min of recovery, slices were transferred to a recording chamber and perfused continuously at 2–4 ml/min with oxygenated ACSF, containing (in mM) 125 NaCl, 25 $NaHCO_3$, 2.5 KCl, 1.25 NaH_2PO_4, 11 glucose, 1.3 $MgCl_2$ and 2.5 $CaCl_2$ at ~30 °C. Cells were visualized with a 40x water-immersion objective on an upright fluorescent microscope (BX51WI; Olympus) equipped with infrared-differential interference contrast video microscopy and epifluorescence (Olympus). Patch pipettes (3.8–4.4 MΩ) were pulled from borosilicate glass (G150TF-4; Warner Instruments) and filled with internal solution, which consisted of (in mM) 130 CsCl, 1 EGTA, 10 HEPES, 2 MgATP, 0.2 NaGTP, 0.1% neurobiotin pH 7.35 (270–285 mOsm). Light-evoked $GABA_A$ mediated IPSCs (Figures 3 and S2) were recorded in the presence of 20 μM CNQX (6-cyano-7-nitroquinoxaline-2,3-dione, Bio-tech) and 50 μM D-AP5 (Tocris) to block AMPA and NMDA receptors, respectively. We also added the voltage-gated sodium channel antagonist tetrodotoxin (TTX, 1 μM, Hello Bio) and the potassium channel antagonist 4-aminopyridine (4-AP, 1 mM, Sigma) to the bath solution in order to isolate monosynaptic inputs (Petreanu et al., 2009). For recordings of light-evoked $GABA_B$ currents (Figures 6A–6F, S6H, S6I and S7B), the internal solution contained (in mM): 115 potassium methylsulfate, 20 NaCl, 1.5 MgCl2, 10 BAPTA, 10 sodium phosphocreatine, 4 MgATP, and 0.4 NaGTP, pH 7.35 (285 mOsm) and cells were recorded in the presence of 50 μM picrotoxin (Sigma), 20 μM CNQX and 50 μM D-AP5. Miniature inhibitory postsynaptic currents (mIPSCs) were recorded in the presence of 1 μM TTX, 20 μM CNQX and 50 μM D-AP5. For recordings of spontaneous firing in VTA dopamine (DA) neurons, the internal solution contained (in mM): 135 K-gluconate, 5 KCl, 10 HEPES, 0.1 EGTA, 2 $MgCl_2$, 2 MgATP, 0.2 NaGTP, and 0.1% neurobiotin, pH 7.35 (290–300 mOsm). Electrophysiological recordings were made at 32 °C using a MultiClamp700B amplifier and acquired using a Digidata 1440A digitizer, sampled at 10 kHz, and filtered at 2 kHz. All data acquisition was performed using pCLAMP software (Molecular Devices). Channelrhodopsin-2 was stimulated by flashing 473 nm light through the light path of the microscope using an ultrahigh-powered light-emitting diode (LED) powered by an LED driver (Prizmatix) under computer control. A dual lamp house adaptor (Olympus) was used to switch between fluorescence lamp and LED light source. The light intensity of the LED was not changed during the experiments and the whole slice was illuminated (5 mW/mm^2). Light-evoked $GABA_A$ responses were obtained every 10 s with one pulse of 473 nm wavelength light (3 ms) with neurons voltage clamped at −70 mV. Light-evoked $GABA_B$ responses were obtained every 30 s with 20 pulses of 473 nm wavelength light (20 Hz, 3 ms) with neurons voltage clamped at −55 mV. mIPSCs were recorded at −70 mV. Series resistance (15–25 MΩ) and input resistance were monitored online. For recordings of spontaneous action potential firing, cells were held in current clamp mode and no current injections were made. Spontaneous firing was recorded for at least 3 s before and 5 s after light stimulation (20 Hz, 3 ms light pulses, 5 mW/mm^2). For pharmacological experiments, we recorded baseline responses and drugs were bath applied for 5–10 min (50 μM picrotoxin to block inhibitory

currents mediated by $GABA_A$ receptors; 100 μM baclofen [Sigma] to activate $GABA_B$ receptors and 100 μM CGP35348 [Sigma] to block $GABA_B$ receptors).

Data were analyzed offline using Clampfit (Molecular Devices) or IgorPro Software (Wavemetrics). Light-evoked IPSC amplitudes were calculated by averaging responses from 10 sweeps and then measuring the peak amplitude in a 50 ms window after the light pulse. Cells that did not show a peak in this window that exceeded the baseline noise were counted as non-responders.

DA and GABA cells were recorded in both the caudal and rostral VTA. The caudal VTA contained at least some parts of the rostromedial tegmental nucleus (RMTg) (Jhou et al., 2009). The boundary between the VTA and RMTg is difficult to determine, particularly in the caudal VTA, which makes it difficult to determine with certainty whether local inhibitory input to VTA DA neurons originates from within the VTA or from the RMTg. Thus, when referred to in the text, the VTA includes the RMTg, which was originally termed the 'tail of the VTA' (Kaufling et al., 2009).

In experiments in which we injected red fluorescent retrobeads into both the NAcLat and NAcMed of the same animal, retrogradely labeled neurons projecting to NAcMed and NAcLat were differentiated according to their anatomical location in the VTA and the presence or absence of an I_h current. NAcMed-projecting DA neurons are mainly located in the mVTA, while NAcLat-projecting DA neurons are predominantly located in the lVTA (Figure 2) (Lammel et al., 2008, 2011). In addition, NAcLat-projecting DA neurons possess a prominent I_h current, which is very small or absent in NAcMed-projecting DA neurons (Lammel et al., 2008, 2011).

To determine the neurochemical identity of retrobead-labeled neurons (i.e. TH-immunopositive or TH-immunonegative), neurons were filled with neurobiotin (Vector) during patch clamp recordings, then fixed in 4% paraformaldehyde (PFA) and 24 h later immunostained for TH. The neurochemical identity was assessed in all experiments (except for experiments shown in Figures 6A–6F) and approximately 80% of all whole-cell patch clamped neurons could be successfully recovered. The DAergic phenotype was confirmed in all of these neurons; a more detailed description on the neurochemical identity of retrogradely labeled neurons in the VTA can be found in Lammel et al., 2011).

BEHAVIORAL ASSAYS

Real-time place preference: Mice with optogenetic implants were connected to a fiberoptic cable and placed in a custom-made behavioral arena (described previously in Lammel et al., 2012; 2015). For optogenetic stimulation, the cable was connected to a 473-nm DPSS laser diode (Laserglow) through an FC/PC adaptor, and laser output was controlled using a Master-8 pulse stimulator (A.M.P.I.). Power output was tested using a digital power meter (Thorlabs) and was checked before and after each experimental animal; output during light stimulation was estimated to be 5–8 mW/mm^2 at the targeted tissue 200 μm from the fiber tip (www.optogenetics.org/calc). One randomly assigned side of the chamber was assigned as the initial stimulation side (Phase 1), and after 10 min the stimulation side was switched to the other previously non-stimulated side of the chamber (Phase 2). At the start of each

session, the mouse was placed in the non-stimulated side of the chamber, and every time the mouse crossed to the stimulation side, 20 Hz (5 ms pulses) constant laser stimulation was delivered until the mouse crossed back into the neutral, non-stimulation side. There was no interruption between Phase 1 and Phase 2. The movement of the mice was recorded via a video tracking system (Biobserve) and the time the mice spent in each area (stimulated, non-stimulated, neutral) was calculated. For optogenetic silencing, mice were continuously stimulated using a 589-nm DPSS laser.

Intracranial self-stimulation: Experimental sessions were conducted in operant conditioning chambers (24 cm W x 20 cm D x 18 cm H, Med Associates Inc.) contained within a sound-attenuating cabinet. The right side of the chamber was fitted with two nosepoke ports, each with an LED light at the rear. Prior to behavioral sessions, mice were gently attached to a fiberoptic patch cord with optical fiber (NA = 0.37, 100 μm diameter, Thorlabs) via a ceramic sleeve (Precision Fiber Products). The patch cable was also connected to a rotary joint (Doric Lenses), which permitted free rotation while transmitting blue light from an upstream 473 nm DPSS laser (Laserglow). Light stimulation was controlled by a computer running Med PC IV software (Med Associates Inc.), which also recorded nosepoke responses. Prior to the test session, the mice spent 5 min in the chamber to habituate to the environment and recover from handling. During this time, all ports were inactive. The start of the session was indicated to the mouse by the illumination of a white house light. Session length was 60 min, during which time mice were free to respond at the two nosepoke ports. One port was designated the “active” port, and a response at this port produced 1 s of light stimulation at 20 Hz. The LED at the back of the port was concurrently illuminated to provide a visual cue signaling the presence of light stimulation. Responses made within the stimulation period were recorded but had no consequence. The second port was designated “inactive”, and responses at this port were recorded but did not result in either light stimulation or cue light presentation. Total number of responses on the active port were compared between ChR2 and eYFP groups. Laser output parameters during light stimulation were the same as in the real-time place preference experiments above.

Open Field Test: The open-field test was conducted to measure the effect of optogenetic stimulation on general locomotor ability. The mice were placed in a custom-made open field chamber (50 × 50 cm) and their movement was recorded and analyzed for 9 min using video-tracking software (Biobserve). The 9-min session was divided into three 3-min epochs; during the first epoch, there was no light stimulation (off), during the second epoch the animal received light stimulation (20 Hz; on), and during the third epoch there was no light stimulation (off). The inner zone of the open-field chamber was defined as the 23 × 23 cm central square area. Light output during stimulation was the same as in the real-time place preference experiments.

Elevated Plus Maze: The elevated plus maze was made of plastic and consisted of two light gray open arms (30 × 5 cm) and two black enclosed arms (30 × 5 cm) extending from a central platform (5 × 5 × 5 cm) at 90 degrees in the form of a plus sign. The maze was placed 30 cm above the floor. Mice were initially placed in the center of the maze and allowed to freely explore, and video tracking software (Biobserve) was used to track their

path. The 9-min session was divided into three 3-min epochs; during the first epoch, there was no light stimulation (off), during the second epoch there was light stimulation at 20 Hz (on), and during the third epoch there was no light stimulation (off). Light output during stimulation was the same as in the real-time place preference experiments, above.

Optopharmacology: Six D1-Cre mice were injected with AAV-DIO-ChR2-eYP into the NAcMed (see stereotactic surgeries for details) and implanted with a custom-made optofluidic system, which allowed precise drug infusion and optogenetic stimulation into the VTA (bregma, −3.4 mm, lateral, 0.5 mm, ventral, −3.8 mm). Mice received unilateral infusion of 1 μL sterile ACSF solution or 15 nM/μL CGP35348 in ACSF into the VTA. Infusions were made at a rate of 0.5 μL/min with a syringe pump (Harvard Apparatus) and were performed in the animal's home cages. After infusion, mice were allowed to spend 3 min in their home cage to allow the drugs to take effect before the behavioral sessions began. We first performed real-time place preference experiments (described above) starting with ACSF infusion, and 24h later CGP35348 infusion experiments were performed. Elevated plus maze experiments were performed 48h later using the procedures outlined above.

HISTOLOGY AND CONFOCAL MICROSCOPY—Immunofluorescence and confocal microscopy were performed as described previously (Lammel et al., 2008, 2012, 2015). Briefly, after intracardial perfusion with 4% paraformaldehyde in PBS, pH 7.4, the brains were post-fixed overnight and coronal midbrain slices (50 or 100 μm) were prepared. The primary antibodies used were rabbit anti-tyrosine hydroxylase (TH, 1:1000, Millipore) and mouse anti-TH (1:1000, Millipore). The secondary antibodies used were Alexa Fluor 546 goat anti-rabbit, Alexa Fluor 546 goat anti-mouse, Alexa Fluor 647 goat anti-rabbit and Alexa Fluor 647 goat anti-mouse (1:750, Thermo Fisher Scientific). Image acquisition was performed with Zeiss LSM710 laser scanning confocal microscope using 20x or 40x objectives and on a Zeiss AxioImager M1 upright widefield fluorescence/differential interference contrast microscope with charge-coupled device camera using 5x objectives. Confocal images were analyzed using ImageJ. Sections were labeled relative to bregma using landmarks and neuroanatomical nomenclature as described in "*The Mouse Brain in Stereotaxic Coordinates*" (Franklin and Paxinos, 2001). For quantification of fluorescence intensities, confocal images were acquired using a 20x objective with identical pinhole, gain and laser settings. 24 images from 3 different animals from medial and lateral VTA and from the same tissue sections were acquired at the same focal level. The medial and lateral VTA was defined as the area that corresponds to the anatomical location of distinct DA subpopulations (Lammel et al., 2008, 2011). The medial VTA was defined as the region comprising the paranigral nucleus and interfascicular nucleus, whereas the lateral VTA was defined as the lateral parabrachial pigmented nucleus and the medial lemniscus adjacent to the substantia nigra. No additional post-processing was performed on any of the collected images. The fluorescence intensity for eYFP and mCherry expression was then quantified in each VTA subregion as the percentage per pixel using ImageJ software.

QUANTIFICATION AND STATISTICAL ANALYSIS

Student's t tests (paired and unpaired), Chi-square test, one-way or two-way ANOVA tests were used to determine statistical differences for anatomical, behavioral and

electrophysiological data using GraphPad Prism 6 (Graphpad Software). Tukey's post hoc test or Holm-Sidak's post hoc analysis was applied when ANOVA showed a significant main effect. Statistical significance was * $p < 0.05$, ** $p < 0.01$, *** $p < 0.001$. All data are presented as means ± SEM. Details of the statistical analysis per figure are summarized in Table S1.

Supplementary Material

Refer to Web version on PubMed Central for supplementary material.

Acknowledgments

We thank the entire Lammel laboratory for helpful discussion, the UNC vector core for the AAV viruses and the CNR Biological Imaging Facility at the University of California, Berkeley. We also thank Robert Zucker, Csaba Földy and Elizabeth Steinberg for critical reading of the manuscript. S.L. is a John P. Stock Faculty Fellow and Rita Allen Scholar. This work was supported by an NIH grant (R01-DA042889), a NARSAD Young Investigator Award (23543) and by the Wayne and Gladys Valley Foundation. H.B. is supported by a Sloan Research Fellowship in Neuroscience and a NARSAD Young Investigator Award.

References

Aragona BJ, Cleaveland NA, Stuber GD, Day JJ, Carelli RM, Wightman RM. Preferential enhancement of dopamine transmission within the nucleus accumbens shell by cocaine is attributable to a direct increase in phasic dopamine release events. J Neurosci. 2008; 28:8821–8831. [PubMed: 18753384]

Bassareo V, De Luca MA, Di Chiara G. Differential expression of motivational stimulus properties by dopamine in nucleus accumbens shell versus core and prefrontal cortex. J Neurosci. 2002; 22:4709–4719. [PubMed: 12040078]

Beier KT, Steinberg EE, DeLoach KE, Xie S, Miyamichi K, Schwarz L, Gao XJ, Kremer EJ, Malenka RC, Luo L. Circuit Architecture of VTA Dopamine Neurons Revealed by Systematic Input-Output Mapping. Cell. 2015; 162:622–634. [PubMed: 26232228]

Berridge KC, Kringelbach ML. Pleasure Systems in the Brain. Neuron. 2015; 86:646–664. [PubMed: 25950633]

Bjorklund A, Dunnett SB. Dopamine neuron systems in the brain: an update. Trends Neurosci. 2007; 30:194–202. [PubMed: 17408759]

Bocklisch C, Pascoli V, Wong JCY, House DRC, Yvon C, de Roo M, Tan KR, Luscher C. Cocaine Disinhibits Dopamine Neurons by Potentiation of GABA Transmission in the Ventral Tegmental Area. Science. 2013; 341:1521–1525. [PubMed: 24072923]

Bromberg-Martin ES, Matsumoto M, Hikosaka O. Dopamine in Motivational Control: Rewarding, Aversive, and Alerting. Neuron. 2010; 68:815–834. [PubMed: 21144997]

Cameron DL, Williams JT. Dopamine D1 receptors facilitate transmitter release. Nature. 1993; 366:344–347. [PubMed: 8247128]

Chuhma N, Tanaka KF, Hen R, Rayport S. Functional Connectome of the Striatal Medium Spiny Neuron. J Neurosci. 2011; 31:1183–1192. [PubMed: 21273403]

Cruz HG, Ivanova T, Lunn ML, Stoffel M, Slesinger PA, Lüscher C. Bi-directional effects of GABAB receptor agonists on the mesolimbic dopamine system. Nat Neurosci. 2004; 7:153–159. [PubMed: 14745451]

Doherty M, Gratton A. Differential involvement of ventral tegmental GABAA and GABAB receptors in the regulation of the nucleus accumbens dopamine response to stress. Brain Res. 2007; 1150:62–68. [PubMed: 17395162]

Dreyer JK, Vander Weele CM, Lovic V, Aragona BJ. Functionally Distinct Dopamine Signals in Nucleus Accumbens Core and Shell in the Freely Moving Rat. J Neurosci. 2016; 36:98–112. [PubMed: 26740653]

Edwards NJ, Tejeda HA, Pignatelli M, Zhang S, McDevitt RA, Wu J, Bass CE, Bettler B, Morales M, Bonci A. Circuit specificity in the inhibitory architecture of the VTA regulates cocaine-induced behavior. Nat Neurosci. 2017; 20:438–448. [PubMed: 28114294]

Eshel N, Tian J, Bukwich M, Uchida N. Dopamine neurons share common response function for reward prediction error. Nat Neurosci. 2016; 19:479–486. [PubMed: 26854803]

Faget L, Osakada F, Duan J, Ressler R, Johnson AB, Proudfoot JA, Yoo JH, Callaway EM, Hnasko TS. Afferent Inputs to Neurotransmitter-Defined Cell Types in the Ventral Tegmental Area. Cell Rep. 2016; 15:2796–2808. [PubMed: 27292633]

Fields HL, Hjelmstad GO, Margolis EB, Nicola SM. Ventral Tegmental Area Neurons in Learned Appetitive Behavior and Positive Reinforcement. Annu Rev Neurosci. 2007; 30:289–316. [PubMed: 17376009]

Gerfen CR, Surmeier DJ. Modulation of striatal projection systems by dopamine. Annu Rev Neurosci. 2011; 34:441–466. [PubMed: 21469956]

Groenewegen HJ, Wright CI, Beijer AV, Voorn P. Convergence and segregation of ventral striatal inputs and outputs. Ann N Y Acad Sci. 1999; 877:49–63. [PubMed: 10415642]

Haber SN, Fudge JL, McFarland NR. Striatonigrostriatal pathways in primates form an ascending spiral from the shell to the dorsolateral striatum. J Neurosci. 2000; 20:2369–2382. [PubMed: 10704511]

Hamid AA, Pettibone JR, Mabrouk OS, Hetrick VL, Schmidt R, Vander Weele CM, Kennedy RT, Aragona BJ, Berke JD. Mesolimbic dopamine signals the value of work. Nat Neurosci. 2015; 19:117–126. [PubMed: 26595651]

Henny P, Brown MTC, Northrop A, Faunes M, Ungless MA, Magill PJ, Bolam JP. Structural correlates of heterogeneous in vivo activity of midbrain dopaminergic neurons. Nat Neurosci. 2012; 15:613–619. [PubMed: 22327472]

Howe MW, Dombeck DA. Rapid signalling in distinct dopaminergic axons during locomotion and reward. Nature. 2016; 535:505–510. [PubMed: 27398617]

Ikemoto S. Dopamine reward circuitry: two projection systems from the ventral midbrain to the nucleus accumbens-olfactory tubercle complex. Brain Res Rev. 2007; 56:27–78. [PubMed: 17574681]

Ikemoto S, Bonci A. Neurocircuitry of drug reward. Neuropharmacology. 2014; 76:329–341. [PubMed: 23664810]

Ikemoto S, Murphy JM, Mcbride WJ. Regional differences within the rat ventral tegmental area for muscimol self-infusions. Pharmacol Biochem Behav. 1998; 61:87–92. [PubMed: 9715810]

Jhou TC, Fields HL, Baxter MG, Saper CB, Holland PC. The Rostromedial Tegmental Nucleus (RMTg), a GABAergic Afferent to Midbrain Dopamine Neurons, Encodes Aversive Stimuli and Inhibits Motor Responses. Neuron. 2009; 61:786–800. [PubMed: 19285474]

Kalivas PW, Duffy P, Eberhardt H. Modulation of A10 dopamine neurons by gamma-aminobutyric acid agonists. J Pharmacol Exp Ther. 1990; 253:858–866. [PubMed: 2160011]

Kalivas PW, Churchill L, Klitenick MA. GABA and enkephalin projection from the nucleus accumbens and ventral pallidum to the ventral tegmental area. Neuroscience. 1993; 57:1047–1060. [PubMed: 7508582]

Kaufling J, Veinante P, Pawlowski SA, Freund-Mercier MJ, Barrot M. Afferents to the GABAergic tail of the ventral tegmental area in the rat. J Comp Neurol. 2009; 513:597–621. [PubMed: 19235223]

Kupchik YM, Brown RM, Heinsbroek JA, Lobo MK, Schwartz DJ, Kalivas PW. Coding the direct/indirect pathways by D1 and D2 receptors is not valid for accumbens projections. Nat Neurosci. 2015; 18:1230–1232. [PubMed: 26214370]

Labouèbe G, Lomazzi M, Cruz HG, Creton C, Luján R, Li M, Yanagawa Y, Obata K, Watanabe M, Wickman K, et al. RGS2 modulates coupling between GABAB receptors and GIRK channels in dopamine neurons of the ventral tegmental area. Nat Neurosci. 2007; 10:1559–1568. [PubMed: 17965710]

Lammel S, Hetzel A, Hackel O, Jones I, Liss B, Roeper J. Unique properties of mesoprefrontal neurons within a dual mesocorticolimbic dopamine system. Neuron. 2008; 57:760–773. [PubMed: 18341995]

Lammel S, Ion DI, Roeper J, Malenka RC. Projection-specific modulation of dopamine neuron synapses by aversive and rewarding stimuli. Neuron. 2011; 70:855–862. [PubMed: 21658580]

Lammel S, Lim BK, Ran C, Huang KW, Betley MJ, Tye KM, Deisseroth K, Malenka RC. Input-specific control of reward and aversion in the ventral tegmental area. Nature. 2012; 491:212–217. [PubMed: 23064228]

Lammel S, Lim BK, Malenka RC. Reward and aversion in a heterogeneous midbrain dopamine system. Neuropharmacology. 2014; 76(Pt B):351–359. [PubMed: 23578393]

Lammel S, Steinberg EE, Földy C, Wall NR, Beier K, Luo L, Malenka RC. Diversity of transgenic mouse models for selective targeting of midbrain dopamine neurons. Neuron. 2015; 85:429–438. [PubMed: 25611513]

Laviolette SR, Van Der Kooy D. GABAA receptors in the ventral tegmental area control bidirectional reward signalling between dopaminergic and non-dopaminergic neural motivational systems. Eur J Neurosci. 2001; 13:1009–1015. [PubMed: 11264674]

Lerner TN, Shilyansky C, Davidson TJ, Evans KE, Beier KT, Zalocusky KA, Crow AK, Malenka RC, Luo L, Tomer R, et al. Intact-Brain Analyses Reveal Distinct Information Carried by SNc Dopamine Subcircuits. Cell. 2015; 162:635–647. [PubMed: 26232229]

Lüscher C. The Emergence of a Circuit Model for Addiction. Annu Rev Neurosci. 2016; 39:257–276. [PubMed: 27145911]

Mahn M, Prigge M, Ron S, Levy R, Yizhar O. Biophysical constraints of optogenetic inhibition at presynaptic terminals. Nature Neuroscience. 2016; 19:554–556. [PubMed: 26950004]

Matsui A, Jarvie BC, Robinson BG, Hentges ST, Williams JT. Separate GABA Afferents to Dopamine Neurons Mediate Acute Action of Opioids, Development of Tolerance, and Expression of Withdrawal. Neuron. 2014; 82:1346–1356. [PubMed: 24857021]

Morales M, Margolis EB. Ventral tegmental area: cellular heterogeneity, connectivity and behaviour. Nat Rev Neurosci. 2017; 18:73–85. [PubMed: 28053327]

Nestler EJ, Carlezon WA. The Mesolimbic Dopamine Reward Circuit in Depression. Biol Psychiatry. 2006; 59:1151–1159. [PubMed: 16566899]

Paladini CA, Roeper J. Generating bursts (and pauses) in the dopamine midbrain neurons. Neuroscience. 2014; 282:109–121. [PubMed: 25073045]

Paladini CA, Celada P, Tepper JM. Striatal, pallidal, and pars reticulata evoked inhibition of nigrostriatal dopaminergic neurons is mediated by GABA A receptors in vivo. Neuroscience. 1999; 89:799–812. [PubMed: 10199614]

Panagis G, Kastellakis A. The effects of ventral tegmental administration of GABA A, GABA B, NMDA and AMPA receptor agonists on ventral pallidum self-stimulation. Behav Brain Res. 2002; 131:115–123. [PubMed: 11844578]

Petreanu L, Mao T, Sternson SM, Svoboda K. The subcellular organization of neocortical excitatory connections. Nature. 2009; 457:1142–1145. [PubMed: 19151697]

Pitman KA, Puil E, Borgland SL. GABA(B) modulation of dopamine release in the nucleus accumbens core. Eur J Neurosci. 2014; 40:3472–3480. [PubMed: 25229321]

Roeper J. Dissecting the diversity of midbrain dopamine neurons. Trends Neurosci. 2013; 36:336–342. [PubMed: 23582338]

Salamone JD, Correa M. The Mysterious Motivational Functions of Mesolimbic Dopamine. Neuron. 2012; 76:470–485. [PubMed: 23141060]

Schultz W. Dopamine reward prediction-error signalling: a two-component response. Nat Rev Neurosci. 2016; 17:183–95. [PubMed: 26865020]

Stamatakis AM, Stuber GD. Activation of lateral habenula inputs to the ventral midbrain promotes behavioral avoidance. Nat Neurosci. 2012; 15:1105–1107. [PubMed: 22729176]

Steinberg EE, Janak PH. Establishing causality for dopamine in neural function and behavior with optogenetics. Brain Res. 2013; 1511:46–64. [PubMed: 23031636]

Sugita S, Johnson SW, North RA. Synaptic inputs to GABAA and GABAB receptors originate from discrete afferent neurons. Neurosci Lett. 1992; 134:207–211. [PubMed: 1350333]

Tan KR, Yvon C, Turiault M, Mirzabekov JJ, Doehner J, Labouèbe G, Deisseroth K, Tye KM, Lüscher C. GABA Neurons of the VTA Drive Conditioned Place Aversion. Neuron. 2012; 73:1173–1183. [PubMed: 22445344]

van Zessen R, Phillips JL, Budygin EA, Stuber GD. Activation of VTA GABA Neurons Disrupts Reward Consumption. Neuron. 2012; 73:1184–1194. [PubMed: 22445345]

Watabe-Uchida M, Zhu L, Ogawa SK, Vamanrao A, Uchida N. Whole-Brain Mapping of Direct Inputs to Midbrain Dopamine Neurons. Neuron. 2012; 74:858–873. [PubMed: 22681690]

Watabe-Uchida M, Eshel N, Uchida N. Neural Circuitry of Reward Prediction Error. Annu Rev Neurosci. 2017; 40:373–394. [PubMed: 28441114]

Westerink BH, Kwint HF, deVries JB. The pharmacology of mesolimbic dopamine neurons: a dual-probe microdialysis study in the ventral tegmental area and nucleus accumbens of the rat brain. J Neurosci. 1996; 16:2605–2611. [PubMed: 8786436]

Willick ML, Kokkinidis L. The effects of ventral tegmental administration of GABAA, GABAB and NMDA receptor agonists on medial forebrain bundle self-stimulation. Behav Brain Res. 1995; 70:31–36. [PubMed: 8519426]

Xi ZX, Stein EA. Nucleus accumbens dopamine release modulation by mesolimbic GABA A receptors—an in vivo electrochemical study. Brain Res. 1998; 798:156–165. [PubMed: 9666112]

Xia Y, Driscoll JR, Wilbrecht L, Margolis EB, Fields HL, Hjelmstad GO. Nucleus Accumbens Medium Spiny Neurons Target Non-Dopaminergic Neurons in the Ventral Tegmental Area. J Neurosci. 2011; 31:7811–7816. [PubMed: 21613494]

Xia Y-F, Margolis EB, Hjelmstad GO. Substance P inhibits GABA $_B$ receptor signalling in the ventral tegmental area: Inhibition of GABA $_B$ by substance P. J Physiol. 2010; 588:1541–1549. [PubMed: 20231139]

Highlights

- Mesolimbic DA subpopulations are embedded within different inhibitory networks
- Distinct NAc inputs promote excitation or inhibition of mesolimbic DA subtypes
- NAc medial shell controls mesolimbic DA subtypes via distinct GABA receptor classes
- NAc lateral shell is a central node of the reward system

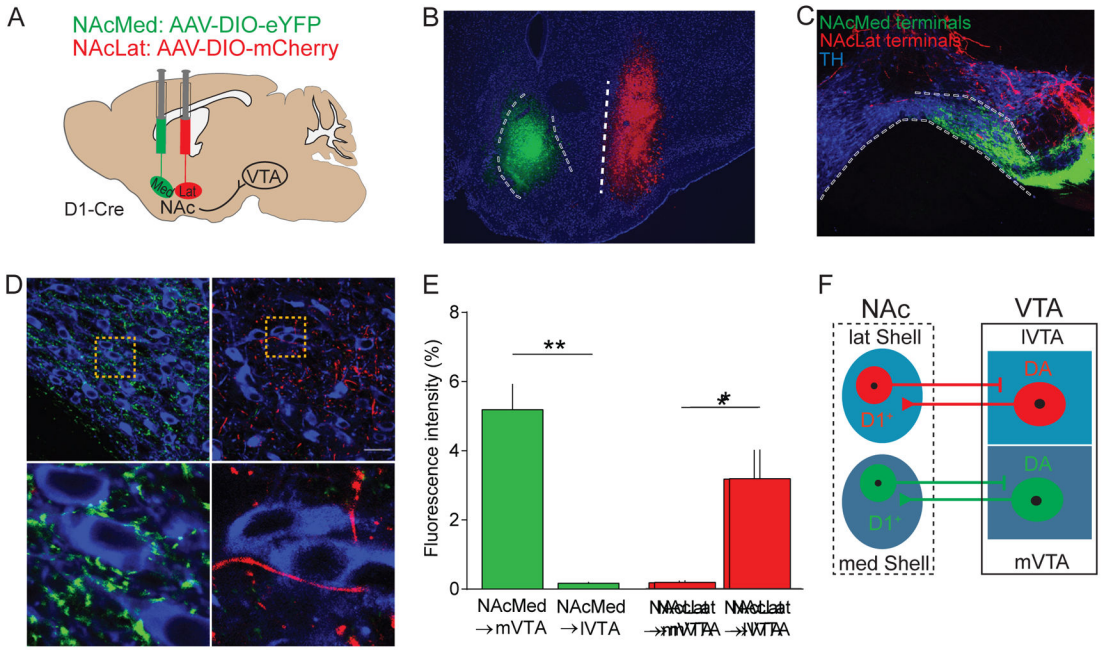

Figure 1. Anatomical characterization of NAcMed and NAcLat inputs to the VTA

(A) Schematic showing dual injection of AAVs expressing eYFP or mCherry into the NAcMed (medial shell of nucleus accumbens) and NAcLat (lateral shell of nucleus accumbens) of D1-Cre mice, respectively.

(B) Fluorescence image showing eYFP expression (green, 488 nm) in the NAcMed and mCherry expression (red, 546 nm) in the NAcLat of a D1-Cre mouse. Blue staining represents DAPI (LV: lateral ventricle, aca: anterior commissure, CPu: caudate putamen, LS: lateral septum, Pir: piriform cortex; Scale bar 100 μm).

(C) Confocal image of a coronal midbrain section showing TH-immunostaining (blue, 647 nm) with eYFP-expressing NAcMed terminals in the medial VTA (mVTA) and mCherry-expressing NAcLat terminals in the lateral VTA (lVTA; IPN: interpeduncular nucleus, ml: medial lemniscus, Scale bar 100 μm).

(D) Confocal images showing dense clustering of eYFP-expressing NAcMed terminals in close proximity of DA neurons in the mVTA (1). mCherry-expressing NAcLat terminals are less frequently observed near DA neurons in the lVTA (2; Scale bars 50 μm).

(E) Bar graphs showing differences in fluorescence intensity for NAcMed and NAcLat terminals in different VTA subregions (* $p < 0.05$, ** $p < 0.01$) (Data represent means ± SEM).

(F) Schematic overview demonstrating matching projection patterns between NAc and VTA subregions.

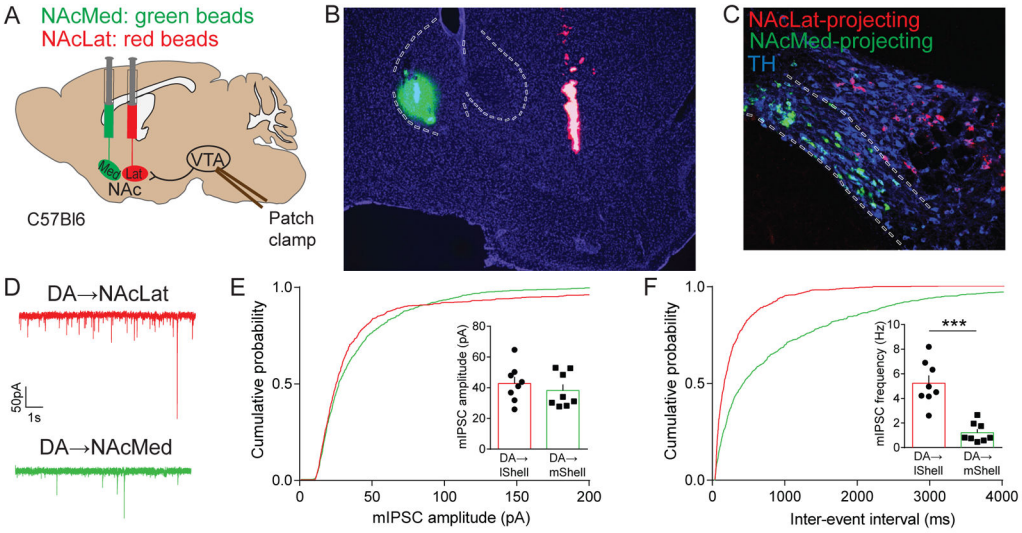

Figure 2. Characterization of inhibitory synaptic transmission in distinct mesolimbic DA subpopulations

(A) Schematic showing dual injection of green and red fluorescent retrobeads into the NAcMed and NAcLat of C57Bl6 mice, respectively, and whole-cell patch clamp recordings of retrogradely labeled VTA DA neurons.

(B) Fluorescence image showing representative example of injection site with green beads located in the NAcMed and red beads in the NAcLat. Blue staining represents DAPI (Scale bar 50 μm).

(C) Confocal image showing TH-immunostaining (647 nm) colocalization with NAcMed-projecting cells in the mVTA (green, 488 nm) and NAcLat projecting cells (red, 546 nm) in the lVTA. ~ 90–97 % of the retrogradely labeled neurons in these regions are TH-immunopositive (i.e., DAergic; Lammel et al., 2011). Note, that NAcMed- and NAcLat-projecting VTA DA neurons represent largely independent projection systems with little collateralization (only 0.4 % of bead-labeled cells harbored both red and green beads (13 out of 3600 cells; red beads: n = 2166 cells, green beads: n = 1421 cells; n = 4 mice) (Scale bar 50 μm).

(D) Example traces of miniature inhibitory postsynaptic currents (mIPSCs) from NAcLat-projecting (red) and NAcMed-projecting (green) VTA DA neurons (recorded in 1 μM TTX, 20 μM CNQX, 50 μM D-AP5).

(E and F) Cumulative probability plots of the amplitudes (E) and frequencies (F) of mIPSCs recorded from NAcLat-projecting (red) and NAcMed-projecting (green) VTA DA neurons. Insets: bar graphs of the means obtained from mIPSC amplitudes (E) or frequencies (F) (*** $p < 0.001$) (Data represent means ± SEM).

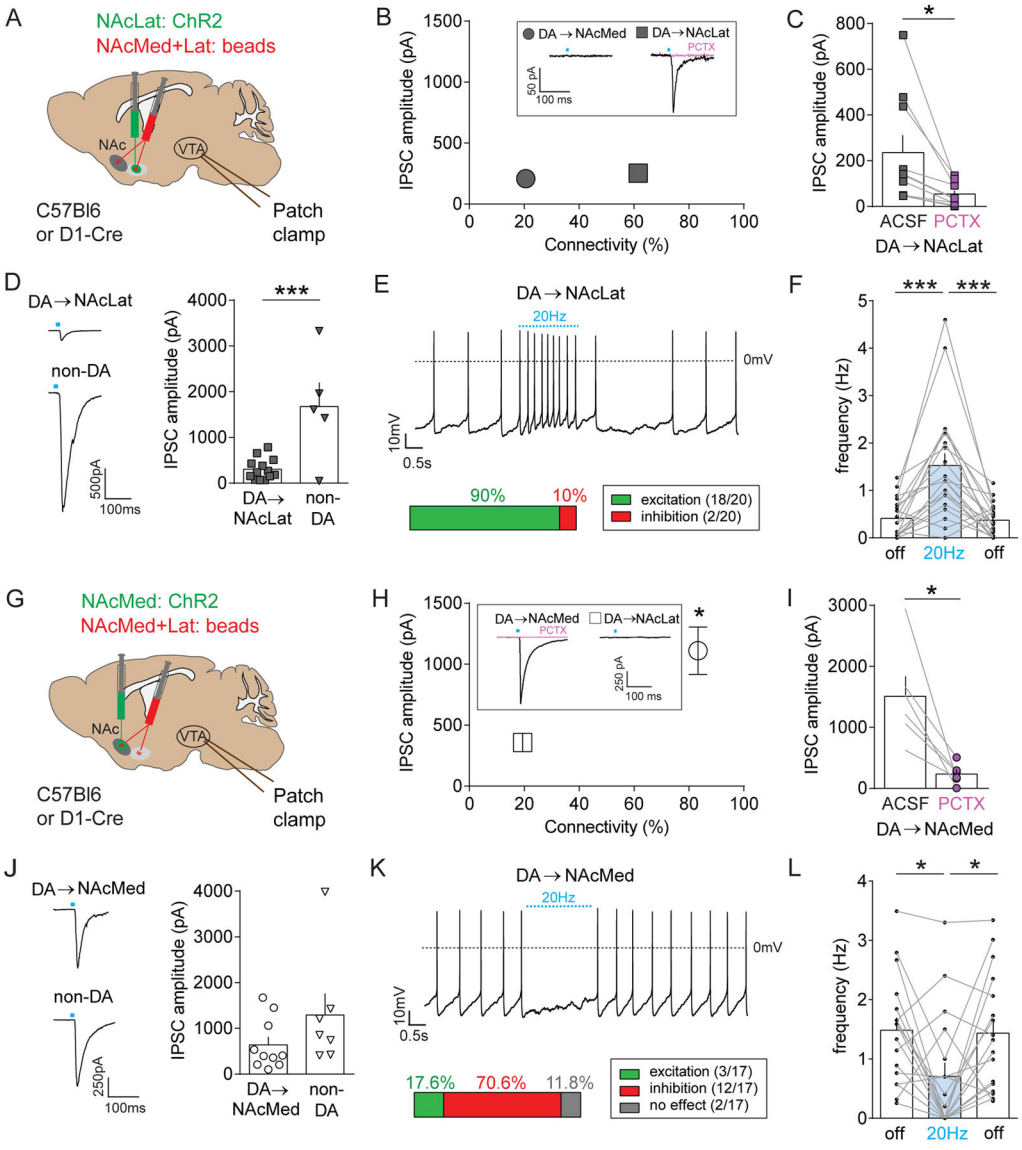

Figure 3. Optogenetic stimulation of discrete NAc inputs to the VTA reveals opposing effects in different mesolimbic DA subpopulations

(A) Schematic of AAV injection into the NAcLat and red retrobead injection into the NAcLat and NAcMed of C57Bl6 (for experiments shown in panels B and C) or D1-Cre mice (for experiments shown in panels D–F). Whole-cell patch clamp recordings were performed from retrogradely labeled neurons in different VTA subregions while optogenetically stimulating NAcLat terminals in the VTA.

(B) Synaptic connectivity plotted against the amplitude of light-evoked inhibitory postsynaptic currents (IPSCs; recorded in 20 μM CNQX, 50 μM D-AP5, 1 μM TTX, 1 mM 4-AP) from NAcMed- (grey circle) and NAcLat-projecting (grey square) DA neurons. Inset shows sample trace of a light-evoked IPSC from a NAcLat-projecting DA neuron (black trace), which are blocked by bath application of 50 μM picrotoxin (red trace). Note that relatively few (~20%) of NAcMed-projecting DA neurons responded to NAcLat terminal stimulation. Error bars are too small to resolve. (Data represent means ± SEM).

(C) Bar graph showing mean IPSC amplitudes before (ACSF) and after bath-application of 50 μM picrotoxin (PCTX) in NAcLat-projecting DA neurons (* $p < 0.05$) (Data represent means ± SEM).

(D) Sample traces showing light-evoked IPSCs recorded in NAcLat-projecting DA neurons and non-DA VTA neurons when stimulating NAcLat terminals in the VTA (left). Bar graph showing significantly larger IPSC amplitudes in non-DA neurons compared to NAcLat-projecting DA neurons (right) (*** $p < 0.001$) (Data represent means ± SEM).

(E) Sample whole-cell patch clamp recording of spontaneous firing in NAcLat-projecting DA neuron and 20 Hz stimulation of NAcLat terminals. Bar chart indicates the percentage of cells that were excited (i.e., increased firing frequency) or inhibited (i.e., decreased firing frequency) in response to NAcLat stimulation.

(F) Bar graph showing the mean firing frequency of NAcLat-projecting DA neurons before (light off), during (light on, 20 Hz) and after (light off) stimulation of NAcLat terminals in the VTA (*** $p < 0.001$) (Data represent means ± SEM).

(G–L) Same experimental approach as in (A–F), but for analyzing NAcMed inputs to NAcLat- and NAcMed-projecting DA neurons. Note the strong synaptic connectivity between the NAcMed and NAcMed-projecting DA neurons (H), the inhibition of light-evoked IPSCs by PCTX (I) and inhibition of spontaneous firing in the majority of NAcMed-projecting DA neurons in response to NAcMed terminal stimulation (K, L) (* $p < 0.05$) (Data represent means ± SEM).

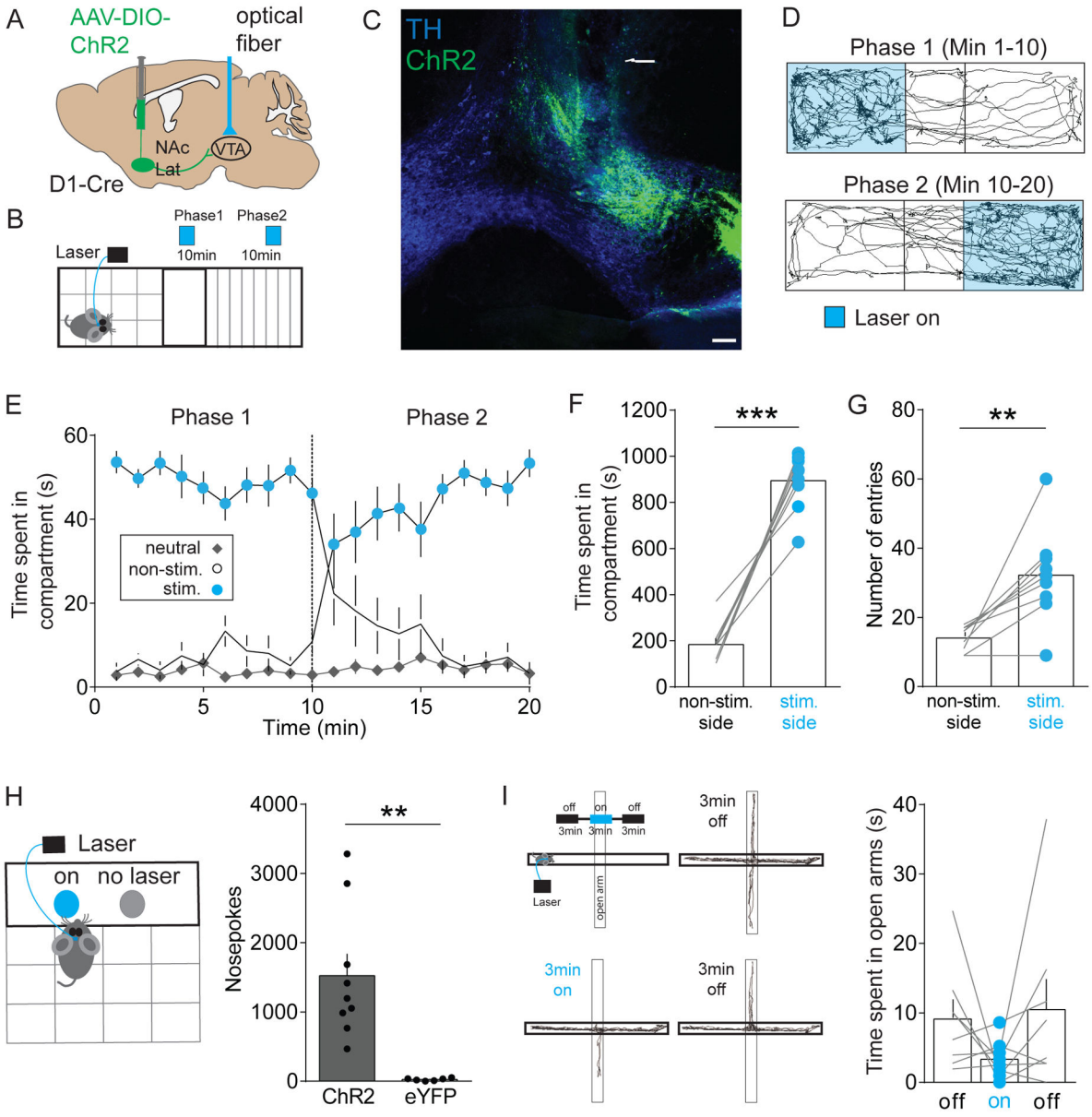

Figure 4. *In vivo* optogenetic stimulation of NAcLat terminals in the VTA promotes reward-related behaviors

(A) Schematic of AAV injection into the NAcLat of D1-Cre mice and light activation of NAcLat terminals in the VTA.

(B) Schematic of real-time place preference assay, which involves switching of light stimulated compartments after 10 min.

(C) Confocal image showing TH-immunostaining (blue, 647 nm), ChR2-eYFP expression in the lVTA (green, 488 nm) and the optical fiber track. Note, that ChR2-eYFP expression is predominantly located in the lVTA (RLi: rostral linear nucleus) (Scale bar 100 μm).

(D) Trajectory of a typical D1-Cre animal that received stimulation in one compartment (Phase 1, blue, top panel) for the initial 10 min period and then received stimulation in the other compartment (Phase 2, blue, lower panel) for an additional 10 min.

(E) Graph showing time spent in individual compartments (neutral: grey; non-stimulated side: white; stimulated side: blue) plotted as a function of time over the course of the experiment (1 min intervals). Dashed line indicates switching of compartment stimulation after 10 min (Data represent means ± SEM).
(F) Mice spend significantly more time on the side of the chamber paired with optical stimulation of NAcLat terminals (*** $p < 0.001$) (Data represent means ± SEM).
(G) Mice enter the side of the chamber paired with optical stimulation of NAcLat terminals more frequently compared to the non-stimulated side (** $p < 0.01$) (Data represent means ± SEM).
(H) Schematic showing behavioral assay in which mice receive optogenetic self-stimulation of NAcLat terminals in the VTA in response to nose-poke behavior (left). Bar graph showing significantly higher nose-poke behavior in mice expressing ChR2 in NAcLat terminals compared to eYFP-expressing animals (right) (** $p < 0.01$) (Data represent means ± SEM).
(I) Schematic of elevated plus maze (EPM) assay, which involves 20 Hz light stimulation of NAcLat terminals in the VTA during a 3-min light-on epoch (upper left panel). Representative trajectory of an animal during the initial 3-min light-off epoch (upper right panel), during the 3-min light-on epoch (lower left panel) and final 3-min light-off epoch (lower right panel). Bar graph showing that light stimulation of NAcLat terminals in the VTA did not significantly alter open arm time compared to light-off epochs (Data represent means ± SEM).

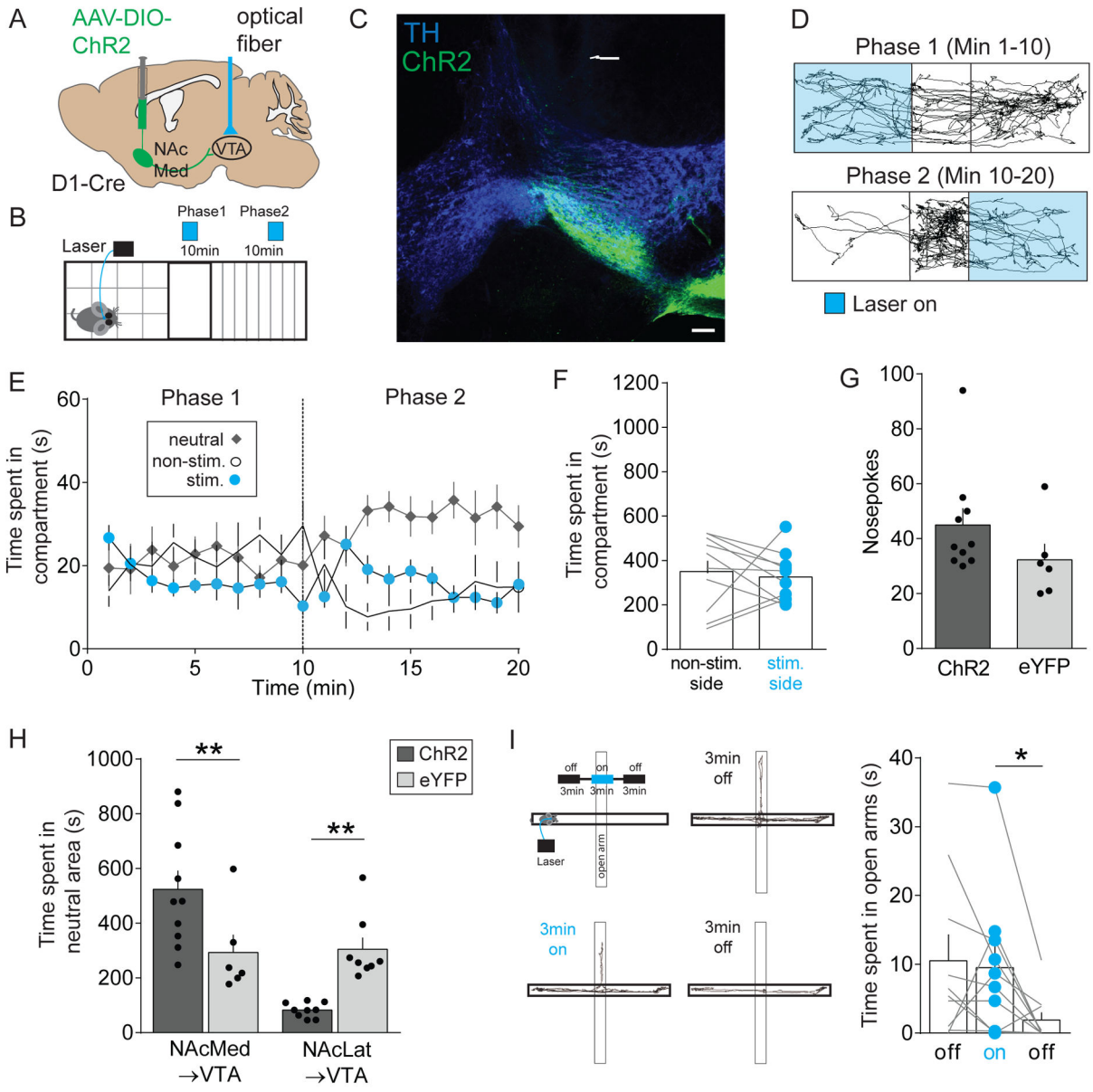

Figure 5. *In vivo* optogenetic stimulation of NAcMed terminals in the VTA induces a general state of behavioral suppression that is not specific to reward or aversion

(A) Schematic of AAV injection into the NAcMed of D1-Cre mice and light activation of NAcMed terminals in the VTA.

(B) Schematic of real-time place preference assay, which involves switching of light stimulated compartments after 10 min.

(C) Confocal image showing TH-immunostaining (blue, 647 nm), ChR2-eYFP expression in the mVTA (green, 488 nm) and the optical fiber track. Note, that ChR2-eYFP expression is predominantly located in the mVTA (Scale bar 100 μm).

(D) Trajectory of a typical D1-Cre animal that received 20 Hz light stimulation in one compartment (Phase 1, blue, top panel) for the initial 10 min period and then received stimulation in the other compartment (Phase 2, blue, lower panel) for an additional 10 min.

(E) Graph showing time spent in individual compartments (neutral: grey; non-stimulated side: white; stimulated side: blue) plotted as a function of time over the course of the experiment (1 min intervals). Dashed line indicates switching of compartment stimulation after 10 min (Data represent means ± SEM).
(F) Optogenetic stimulation of NAcMed terminals in the VTA did not significantly alter the time spent in the stimulated compartment compared to the non-stimulated side (Data represent means ± SEM).
(G) Bar graph showing that optogenetic stimulation of NAcMed terminals in the VTA did not significantly change nose-poke behavior in mice ChR2- compared to eYFP-expressing animals (Data represent means ± SEM).
(H) Bar graph showing that mice receiving optogenetic stimulation of NAcMed terminals in the VTA spent significantly more time in the neutral compartment compared to eYFP-expressing animals or mice that express ChR2 or eYFP in NAcLat terminals (* < 0.05, *** $p < 0.001$) (Data represent means ± SEM).
(I) Schematic of elevated plus maze (EPM) assay, which involves 20 Hz light stimulation of NAcMed terminals in the VTA during a 3-min light-on epoch (upper left panel). Representative path of an animal during the initial 3-min light-off epoch (upper right panel), during the 3-min light-on epoch (lower left panel) and final 3-min light-off epoch (lower right panel). Bar graph showing that light stimulation of NAcMed terminals in the VTA significantly reduced open arm time during the final 3-min light-off epochs (* $p < 0.05$) (Data represent means ± SEM).

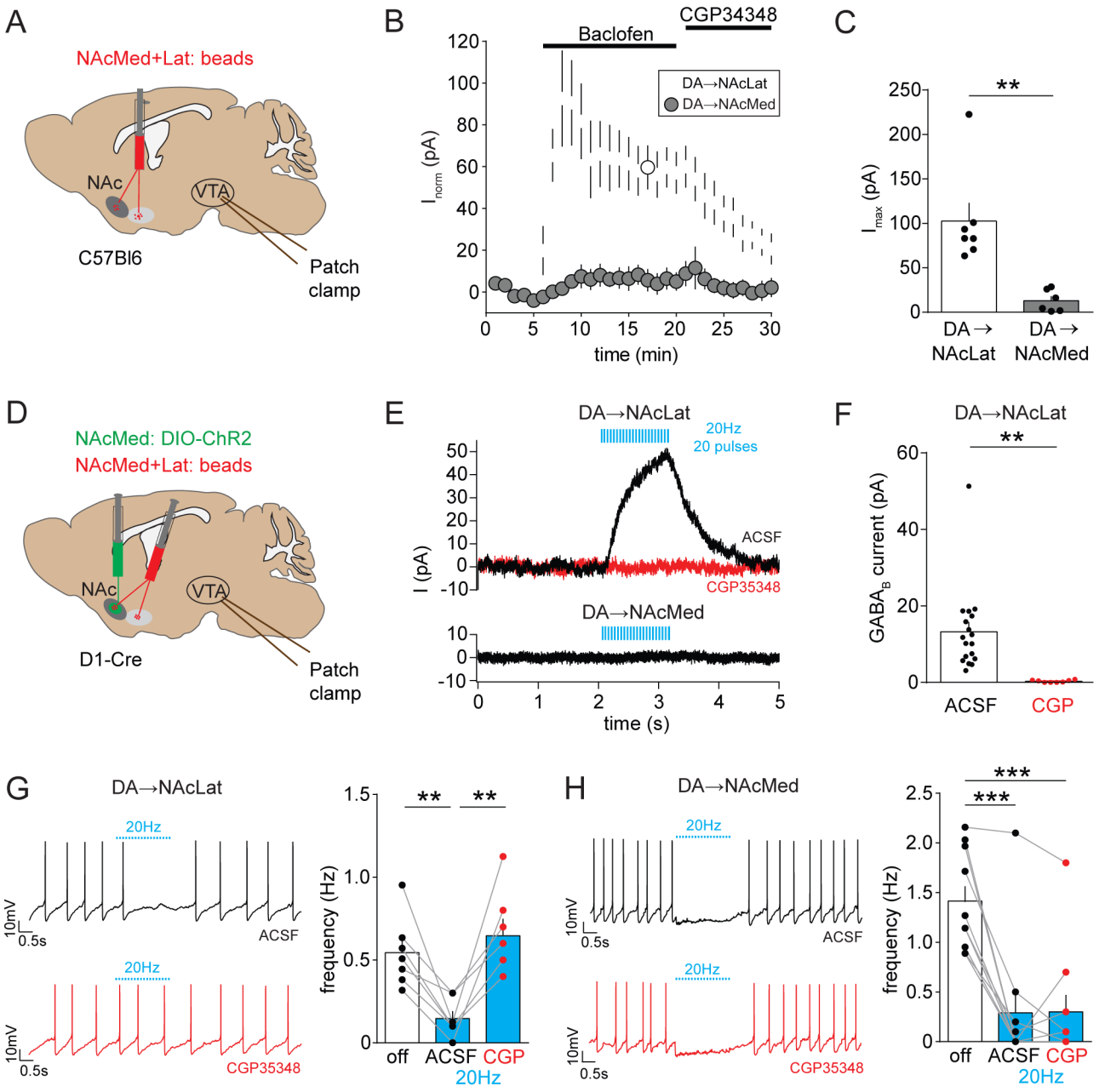

Figure 6. Optogenetic stimulation of NAcMed terminals in the VTA elicits $GABA_B$ receptor activation selectively in NAcLat-projecting VTA DA neurons

(A) Experimental approach showing dual injection of red fluorescent beads into the NAcMed and NAcLat of the same C57Bl6 mouse and *ex-vivo* whole-cell recordings of retrogradely labeled VTA neurons.

(B) Outward currents (recorded at −55 mV, in 50 μM picrotoxin, 20 μM CNQX, 50 μM D-AP5) are plotted as a function of time for NAcLat-projecting DA neurons (white circles) and NAcMed-projecting DA neurons (grey circles). Bath application of 100 μM baclofen (GABABR agonist) induces a striking increase in outward current in NAcLat-projecting but not NAcMed-projecting DA neurons. Note that the baclofen-induced current is blocked by

bath application of the GABABR antagonist CGP35348 (100 μM) (Data represent means ± SEM).

(C) Bar graph showing significantly reduced peak outward currents evoked by baclofen in NAcMed-projecting DA neurons compared to NAcLat-projecting DA neurons (** $p < 0.01$) (Data represent means ± SEM).

(D) Schematic of AAV injection into NAcMed and red retrobead injection into NAcMed and NAcLat of D1-Cre mice. Whole-cell patch clamp recordings were performed from retrogradely labeled neurons in different VTA subregions while stimulating NAcMed terminals in the VTA.

(E) Representative voltage-clamp recording of a NAcLat-projecting DA neuron (upper panel) and NAcMed-projecting DA neuron (lower panel) held at −55 mV (recorded in 50 μM picrotoxin, 20 μM CNQX, 50 μM D-AP5) showing outward current produced by 20 Hz light stimulation of NAcMed terminals. Red trace indicates outward current after application of 100 μM CGP35348.

(F) Bar graph showing mean GABABR-mediated current amplitudes before (ACSF) and after bath-application of CGP35348 (CGP) in NAcLat-projecting DA neurons (** $p < 0.01$) (Data represent means ± SEM).

(G) Left: Sample whole-cell patch clamp recordings of spontaneous firing from a NAcLat-projecting DA neuron and 20 Hz light stimulation of NAcMed terminals before (black trace) and after (red trace) bath application of 100 μM CGP35348. Right: Bar graph showing the mean firing frequency of NAcLat-projecting DA neurons before (off, white bar) and during 20 Hz light stimulation (blue bars) of NAcMed terminals in the VTA (** $p < 0.01$) (Data represent means ± SEM).

(H) Same as in (G), but recordings were performed from NAcMed-projecting DA neurons (*** $p < 0.001$) (Data represent means ± SEM).

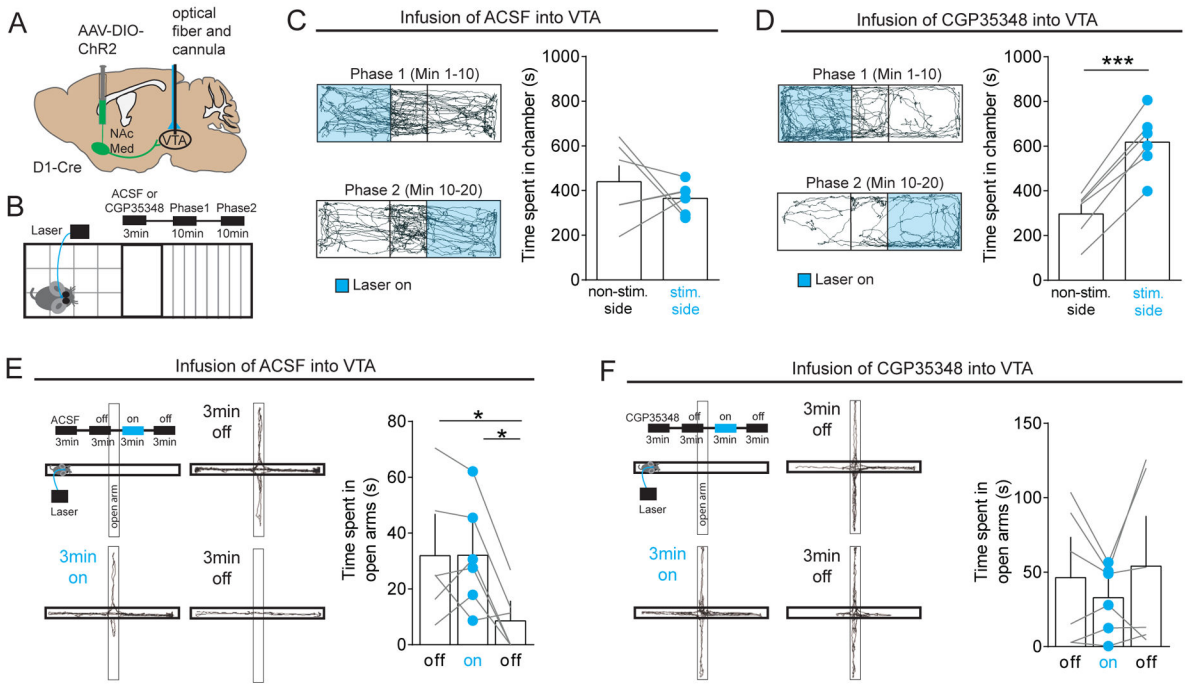

Figure 7. ***In vivo*** **opto-pharmacological dissection of NAcMed projections to the VTA**

(A) Schematic of AAV injection into the NAcMed of D1-Cre mice and implantation of an optofluidic system in the VTA.

(B) Schematic showing experimental approach, which involves infusion of 1μL ACSF or a GABABR antagonist (15 nM/1 μL CGP35348) 3 min before the behavioral assay and two 10 min real-time place preference sessions (light stimulated compartments were switched after 10 min) stimulating NAcMed terminals in the VTA.

(C) Trajectory of a typical D1-Cre animal that received ACSF infusion into the VTA and 20 Hz light stimulation in one compartment (Phase 1, blue, top panel) for the initial 10 min period followed by stimulation in the other compartment (Phase 2, blue, lower panel) for an additional 10 min. Bar graph (right panel) shows that optogenetic stimulation of NAcMed terminals in the VTA did not significantly alter the time spent in the stimulated compartment compared to the non-stimulated side (Data represent means ± SEM).

(D) Same as in (C) but animals received infusion of CGP35348 into the VTA. Note that mice spent significantly more time on the side of the chamber paired with optical stimulation of NAcMed terminals (** $p < 0.01$) (Data represent means ± SEM).

(E) Schematic showing infusion of ACSF into the VTA and elevated plus maze (EPM) assay in which mice received 20 Hz light stimulation of NAcMed terminals during a 3-min light-on epoch (upper left panel). Representative trajectory of an animal during the initial 3-min light-off epoch (upper right panel), during the 3-min light-on epoch (lower left panel) and during the final 3-min light-off epoch (lower right panel). The bar graph shows that light stimulation of NAcMed terminals in the VTA significantly reduced open arm time during the final 3-min light-off epochs (* $p < 0.05$) (Data represent means ± SEM).

(F) Same as in (E) but animals received infusion of CGP35348 into the VTA. Note that mice spent a similar amount of time in the open arms in the two 3-min light-off epochs (Data represent means ± SEM).

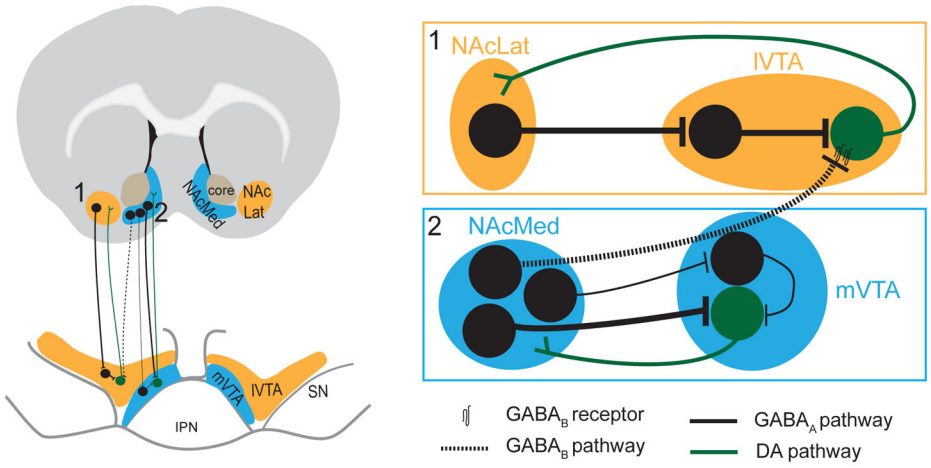

Figure 8. Wiring diagram illustrating direct and indirect feedback loops in the mesolimbic DA system

Our data suggest that the mesolimbic DA system contains both indirect (1) and direct (2) feedback loops. Indirect: D1-expressing medium spiny neurons (MSNs) in the NAcLat predominantly target VTA GABA neurons, which exert inhibitory influence over NAcLat-projecting DA neurons. Thus, activation of the NAcLat pathway increases firing of NAcLat-projecting DA neurons through a net disinhibition. There also appears to be an indirect pathway from D1-expressing MSNs in the NAcMed to mVTA GABA neurons, which inhibit NAcMed-projecting DA neurons. However, NAcMed terminal stimulation in the VTA resulted in a net inhibition in most NAcMed-projecting DA neurons suggesting that the direct pathway from D1-expressing MSN in NAcMed to NAcMed-projecting DA neurons is stronger compared to the indirect pathway. Direct: D1-expressing MSNs in the NAcMed directly inhibit NAcMed-projecting DA neurons via GABAARs and NAcLat-projecting DA neurons via GABABRs. Thus, activation of the NAcMed pathway results in inhibition of both NAcMed- and NAcLat-projecting DA neurons.